PHYSICS REPORTS (Section C of Physics Letters) 18, no. 2 (1975) 125–158. NORTH-HOLLAND PUBLISHING COMPANY

A STUDY OF THE NUCLEAR RESPONSE FUNCTION*

G.F. BERTSCH and S.F. TSAI

Dept. of Physics and Cyclotron Laboratory, Michigan State University, East Lansing, Michigan 48824, USA

Received 1 September 1974

Contents:

Abstract:

We examine the excitation properties of spherical nuclei in the Random Phase Approximation using the Green's function method. The calculations are done with interactions of the Skyrme type for nuclei from ^{16}O to ^{208}Pb. Different Skyrme interactions can have the same predictions for ground state Hartree–Fock properties, but give quite different predictions for the dynamic response. Our calculations favor a mild velocity-dependence in the interaction, such as given by Skyrme I. The level of agreement with empirical properties is as follows: energies of low-lying states, ~25%; positions of giant resonances, ~10%; transition rates of low states, factor of 2 typical. Inelastic scattering of electrons is reasonably accounted for by the model, but nucleon inelastic scattering has difficulties with the noncollective strength.

Single orders for the issue

PHYSICS REPORTS (Section C of PHYSICS LETTERS) 18, No. 2 (1975) 125–158.

Copies of this issue may be obtained at the price given below. All orders should be sent directly to the Publisher. Orders must be accompanied by check.

Single issue price Dfl. 12.50, postage included.

* Supported by the National Science Foundation.

A STUDY OF NUCLEAR RESPONSE FUNCTION

G.F. BERTSCH and S.F. TSAI

Dept. of Physics and Cyclotron Laboratory,
Michigan State University, East Lansing, Michigan 48824, USA

1. Introduction

We describe here a technique for calculations of nuclear properties which is quite different from the usual. The standard method in nuclear physics is to construct wavefunctions in the Schrödinger representation, and use these wavefunctions explicitly to calculate observables. The shell model provides a representation of the wavefunction in the space of single particle nucleon configurations. Although the technique has been highly successful, certain limitations are evident:

First, the region of excitation energy that can be handled is limited. States at high excitation are closely spaced and are not true eigenstates.

Second, the theory is not really a many-body theory in the sense that the limit of a large number of particles is not built in. To really understand nuclei, we should have a theory that separates the true many-body aspects of the dynamics from the uninteresting peculiarities of specific shell structure.

Finally, by the representation in shell model space, a great deal of the physics is obscured in the sheer numerics of the wavefunction vectors. Coordinate space would be much more useful if it could be exploited. For example, it is obvious that for static properties, the density function $\rho(r)$ is more useful than an enumeration of the shell model components of the wavefunction.

A theory which overcomes these defects to some extent is the linear response theory developed for the general many-body problem. The basic object of the theory is the particle–hole Green's function, $G(r_1, r_2, E)$. This is formally defined as

$$G(r_1, r_2, E) = \mathrm{i} \int \mathrm{d}t \, \mathrm{e}^{\mathrm{i}Et} \langle 0 | T\{a^+(r_1, t) a(r_1, t) a^+(r_2, 0) a(r_2, 0)\} | 0 \rangle \tag{1}$$

where $a(r, t)$ and $a^+(r, t)$ are particle annihilation and creation operators in the Heisenberg representation. This is also called the density–density correlation function, since the operator product $a^+(r, t) a(r, t)$ measures the density at point r and time t. The formal definition and basic properties of this Green's function are expounded in standard textbooks on many-body theory [1].

An alternate representation of G, in terms of the Schrödinger eigenstates ψ_n and eigenenergies E_n, is given by

$$G(r_1, r_2, E) = \sum_n \langle \psi_0 | a^+(r_1) a(r_1) | \psi_n \rangle \langle \psi_n | a^+(r_2) a(r_2) | \psi_0 \rangle \left\{ \frac{1}{E_n - E_0 - E - \mathrm{i}\epsilon} + \frac{1}{E_n - E_0 + E - \mathrm{i}\epsilon} \right\}, \tag{2}$$

assuming time-reversal invariance of the matrix elements.

Some useful properties of G can be easily discovered from this representation:

i) the poles of G are the natural resonances of the system, i.e. the excited states;

ii) an external field of the form $f(r) \exp(-\mathrm{i}Et)$ induces a density oscillation given by

$$R_E(f, r) = \int \mathrm{d}^3 r' \, G(r, r', E) f(r') \,. \tag{3a}$$

This is the response function for the field f. The transition strength out of $|0\rangle$ induced by f is

$$\sum_n |\langle n | f | 0 \rangle|^2 \, \delta(E_n - E_0 - E) = \frac{1}{\pi} \int \mathrm{d}^3 r \, \mathrm{d}^3 r' \, f^*(r) \, \mathrm{Im} \, G(r, r', E) f(r') \,; \tag{3b}$$

iii) inelastic scattering in the Born approximation is given by the simple formula [2]

$$\frac{d\sigma}{dq\,dE} = \frac{1}{\pi}\mathrm{Im}\int R_E(e^{iq\cdot r}, r)\, e^{-iq\cdot r}\, d^3r \frac{d\sigma^{el}}{dq} \tag{4}$$

where q is the momentum transfer, E is the energy loss of the projectile, and $d\sigma^{el}/dq$ is the elastic projectile–nucleon scattering cross section.

Direct calculation of G is possible in the standard many-body approximation known as RPA. Various forms of RPA have been used in nuclear physics over the last decade, beginning with the work of Ferrel [3], Baranger [4], and others [5]. Both early [6] and recent [7] derivations of RPA have been given with Green's function formalism, but all actual calculations have been carried out in an occupation number representation. In principle there is no new physics in the use of G directly, since it can always be extracted from the occupation number representation with eq. (2). We pursue RPA calculations in the Green's function representation at this time for two reasons.

The first reason, alluded to above, is that we are able to keep the calculation in coordinate space. This makes it numerically simpler than a theory in the space of single-particle configurations, if the size of the matrix needed to represent this function of two space variables is smaller than the dimension of the shell model space needed to describe the configurations. This is indeed the case for the heavier nuclei that are considered below. This was shown by Blomqvist [8], who used coordinate space to calculate properties of ^{208}Pb. However, he retained much of the occupation number formalism and so was led to calculation of unnecessary state vectors. Much of physics is best visualized and formulated in coordinate space. As we shall see, the coordinate space representation facilitates calculations of such dynamic properties as total inelastic cross sections or medium polarization effects on the residual interaction between valence nucleons. But surely there must be a catch somewhere. There is, and it is that we are only able to deal with exchange interactions in short-range approximations. This will become clear later.

The second reason for pursuing the study concerns the dependence of RPA on Hartree–Fock theory. Bona fide RPA can only be done given a Hartree–Fock theory, and it is only recently that Hartree–Fock theories have been put forth which are both manageable [9,10] and justified to a large extent from the fundamental nucleon interaction [11]. Fortunately for us, these theories treat exchange in a short-range approximation. Previously, RPA calculations have not been based on a Hartree–Fock model. A consistent treatment of the ground state and vibrations should provide a powerful test of the Hamiltonian, and could distinguish between different models, or even invalidate the entire Hartree–Fock theory.

In this article we shall calculate the simple properties of spherical nuclei accessible from the response function; namely, the location and distribution of excitation strength. As reported in a preliminary article [32], we find that the predicted dynamics usefully distinguish between different Hartree–Fock theories having the same ground state properties. The theories emphasizing density-dependence as opposed to the velocity dependence of the effective interaction give good agreement on isoscalar properties and should be applied to more complicated questions. On the other hand, the isovector properties of nuclei seem to be inadequately modeled by the Hartree–Fock RPA treatment.

The plan of this article is the following. We first review the RPA formalism in coordinate space and describe the numerical realization of the integral equations. We then consider general features of the theory, sum rules and form factors. Finally, we present results of calculations with different Hamiltonians for the states and strength functions of a variety of nuclei.

2. Formalism

We shall first derive the equations we use for the RPA Green's function, using time-dependent Hartree–Fock theory. The derivation has been given many times before [3, 12], but for continuity, it is useful to sketch it in the Green's function formalism. Readers familiar with the formalism may just note the operational equation, eq. (19), and go on to the next section.

The Hartree–Fock theory is based on a single-particle Hamiltonian,

$$H = T + V[\rho] + V_{\text{exch}} \tag{5}$$

which in turn is based on some Hamiltonian density. For the single-particle potential V, we have explicitly separated a local part, with some functional dependence on the density ρ, and an exchange interaction, V_{exch}. Eventually we will allow the local part of V to depend on current densities and derivatives of the mass density as well as ρ itself. The exchange interaction V_{exch} is nonlocal, and it is not possible to treat it with local Green's functions in general. As mentioned before, it will be treated in a local approximation. To completely specify the static Hartree–Fock theory, we write down the equation for the single-particle wave-functions ϕ_i and energies ϵ_i,

$$H[\rho]\,\phi_i = \epsilon_i \phi_i \tag{6}$$

and the definition of the density

$$\rho = \sum_{\substack{i \\ \text{occupied}}} \phi_i^* \phi_i \,. \tag{7}$$

In the time dependent theory, we add an external field to H of the form

$$e^{-i\omega t} V_{\text{ext}}(r) + \text{H.C.}$$

This must produce a density perturbation with the same time dependence,

$$\rho = \rho_0 + (\rho' e^{-i\omega t} + \text{H.C.}) \tag{8}$$

where ρ_0 is the unperturbed Hartree–Fock density. According to eqs. (1) and (3a), the Green's function is just the operator function relating $\rho'(r)$ to $V_{\text{ext}}(r')$.

We now construct a Hartree–Fock theory with wavefunctions that allow a density oscillation of $e^{\pm i\omega t}$. The single-particle wavefunction must be of the following form:

$$\phi_i = \phi_i^0 + e^{-i\omega t}\,\phi_i' + e^{+i\omega t}\phi_i'' \tag{9}$$

where we may take ϕ', ϕ'' orthogonal to ϕ^0. This implies to first order

$$\langle \phi_i | \phi_i \rangle = \langle \phi_i^0 | \phi_i^0 \rangle = 1 \,.$$

The new Hartree–Fock Hamiltonian is

$$H(t) = H_0 + \left(e^{-i\omega t} V_{\text{ext}} + e^{-i\omega t}\, \frac{\delta V}{\delta \rho}\, \rho' + \text{H.C.} \right) \tag{10}$$

and the new Hartree–Fock equations are

$$\left\{H_0 + \left(e^{-i\omega t} V_{ext} + e^{-i\omega t} \frac{\delta V}{\delta \rho}\ \rho' + \text{H.C.}\right) - \epsilon_i\right\} \phi_i = i \frac{d}{dt} \phi_i \tag{11}$$

with $H_0 = H[\rho_0]$. The coefficients of $e^{i\omega t}$ and $e^{-i\omega t}$ in these equations satisfy

$$\begin{aligned} &(H_0 - \epsilon_i)\,\phi_i' + \left(V_{ext} + \frac{\delta V}{\delta \rho}\ \rho'\right)\phi_i^0 = +\omega \phi_i' \qquad (e^{-i\omega t}) \\ &(H_0 - \epsilon_i)\,\phi_i'' + \left(V_{ext}^{+} + \frac{\delta V^{+}}{\delta \rho}\ \rho'^{*}\right)\phi_i^0 = -\omega \phi_i'' \qquad (e^{+i\omega t})\ . \end{aligned} \tag{12}$$

In addition, we have

$$\rho' = \sum_{\text{occupied}} (\phi_i' \phi_i^{0*} + \phi_i''^{*} \phi_i^0)\ . \tag{13}$$

We solve these equations for ϕ_i' and ϕ_i'' by formally dividing $H_0 - \epsilon_i \pm \omega$. Thus,

$$\phi_i' = \frac{-1}{H_0 - \epsilon_i - \omega} \left(V_{ext} \phi_i^0 + \frac{\delta V}{\delta \rho}\ \rho' \phi_i^0\right) \tag{14a}$$

$$\phi_i'' = \frac{-1}{H_0 - \epsilon_i + \omega} \left(V_{ext}^{+} \phi_i^0 + \frac{\delta V^{+}}{\delta \rho}\ \rho'^{*} \phi_i^0\right)\ . \tag{14b}$$

Using eqs. (13) and (14) we have

$$\rho' = -\sum_i \phi_i^{0*} \left\{\frac{V_{ext} + (\delta V/\delta \rho)\rho'}{H_0 - \epsilon_i - \omega} + \frac{V_{ext} + \rho'(\delta V/\delta \rho)}{H_0 - \epsilon_i + \omega}\right\} \phi_i^0\ . \tag{15}$$

We now define a bare Green's function,

$$G_{\pm}^{(0)}(r_1, r_2, \omega) = \sum_i \phi_i^{0*}(r_1) \left[\frac{1}{H_0 - \epsilon_i - \omega} + \frac{\pm 1}{H_0 - \epsilon_i + \omega}\right] \phi_i^0(r_2)\ . \tag{16}$$

The single particle operator expression, $1/(H_0 - \epsilon_i - \omega)$, can be given a useful form by expanding in the eigenstates of H_0, which of course are just the Hartree–Fock orbits,

$$\frac{1}{H_0 - \epsilon_i - \omega} = \sum_m \phi_m^{*}(r) \frac{1}{\epsilon_m - \epsilon_i - \omega}\ \phi_m(r')\ .$$

Then the expression for $G^{(0)}$ has the computable form,

$$G_{\pm}^{(0)} = \sum_{i,m} \phi_i^{0*}(r_1)\, \phi_m^0(r_1) \left[\frac{1}{\epsilon_m - \epsilon_i - \omega} + \frac{\pm 1}{\epsilon_m - \epsilon_i + \omega}\right] \phi_m^{0*}(r_2)\, \phi_i^0(r_2)\ . \tag{17}$$

Then we can write eq. (15) in the form

$$\rho' = -\sum_{\pm} G_{\pm}^{(0)} \tfrac{1}{2} \left\{(V_{ext} \pm V_{ext}^{+}) + \left(\frac{\delta V}{\delta \rho} \pm \frac{\delta V^{+}}{\delta \rho}\right)\rho'\right\}\ . \tag{18}$$

The solution of this equation for ρ' is

$$\rho' = -G^{\mathrm{RPA}} V_{\mathrm{ext}}$$

with

$$G^{\mathrm{RPA}} = G^{(0)} \left(1 + \frac{\delta V}{\delta \rho}\, G^{(0)}\right)^{-1} . \tag{19}$$

Here the sum over ± indices is implicit. This is the fundamental equation of the theory.

$G^{(0)}$ has been given an explicit coordinate space representation and as long as $\delta V/\delta\rho$ has a simple form also, eq. (19) will be calculable. We notice that the basic two-body interaction is the functional derivative of the Hartree–Fock Hamiltonian with respect to density. This form is not completely obvious when the basic Hamiltonian density has multiparticle interactions, but is absolutely necessary for the consistency of the theory [13].

3. Interactions

As mentioned in the introduction, Hartree–Fock calculations are possible in a simple way with a certain class of interactions introduced by Skyrme [14]. The essential features of the interaction $V(r)$ is that it contains derivatives of no higher order than second and that it depends only on densities and derivatives at a given point. Thus it has zero range and exchange can be included exactly. This is not only a simplification for Hartree–Fock, but enables the RPA to be done exactly with a simple set of Green's functions. The most general potential energy density for a central interaction with these specifications is,

$$\mathcal{V} = A[\rho_{\sigma\tau}] + B[\rho_{\sigma\tau}]\langle p^2\rangle + B'[\rho_{\sigma\tau}] \sum_{i<j} \boldsymbol{p}_i \cdot \boldsymbol{p}_j + E[\rho_{\sigma\tau}]\ \nabla\rho \cdot \nabla\rho . \tag{20}$$

In this equation, $\boldsymbol{p}$ is the momentum density, A, B, B', E are functions of the density at the same point, and $\rho_{\sigma\tau}$ is the density of nucleons with spin, isospin projections $S_z = \sigma$, $T_z = \tau$. The Skyrme form has four parameters t_0, t_1, t_2, t_3, and x, with the potential energy a quadratic and cubic function of density. The functions in eq. (20) for the Skyrme interaction are given in table 1. The Skyrme interaction has in addition a spin–orbit term; this is unimportant in the dynamics and we neglect it. The tensor interaction can be included in this potential but has not been to date. For a Galilean-invariant interaction, $B' = -B/\rho$. The potential given by Negele and Vautherin [11] is of this form but without an explicit B' term.

With the above potential energy density, the Hartree–Fock Hamiltonian has the form

$$H = \frac{\delta(\langle p^2\rangle/2m + \mathcal{V})}{\delta\rho} = -\frac{\hbar^2}{2m}\nabla^2 + V = -\nabla\cdot\left(\frac{\hbar^2}{2m} + B\right)\nabla$$
$$+\left[\frac{\delta A}{\delta\rho} + \frac{\delta B}{\delta\rho}\langle p^2\rangle - \left(\frac{\delta E}{\delta\rho} + \frac{1}{4}\frac{\delta^2 B}{\delta\rho^2}\right)(\nabla\rho)^2 - \left(2E + \frac{1}{4}\frac{\delta B}{\delta\rho}\right)\nabla^2\rho\right] - \left[\frac{B}{\rho}\langle p\rangle\cdot p + \langle p\rangle\cdot\langle p\rangle\frac{\delta(B/\rho)}{\delta\rho}\right]. \tag{21}$$

The last term vanishes in the Hartree–Fock ground state, because the expectation value of the current is zero, but it will contribute to the RPA Green's function when we take the functional derivative of the Hartree–Fock potential V.

Table 1
Coefficients of the RPA Hamiltonian density (eq. (20)), with the Skyrme interaction. Noncentral interactions are neglected, and exchange is implicit.

$$A = \tfrac{1}{2}t_0[\tfrac{3}{4}(\rho_n+\rho_p)^2 - (\tfrac{1}{4}+\tfrac{1}{2}x_0)(\rho_n-\rho_p)^2] + \tfrac{1}{4}t_3\rho_n\rho_p(\rho_n+\rho_p)$$

$$B\langle p^2\rangle = \tfrac{1}{16}(3t_1+5t_2)(\rho_n+\rho_p)(\langle p^2\rangle_n+\langle p^2\rangle_p) + \tfrac{1}{16}(t_2-t_1)(\rho_n-\rho_p)(\langle p^2\rangle_n-\langle p^2\rangle_p)$$

$$E(\nabla\rho)^2 = \tfrac{1}{64}(3t_1-15t_2)\nabla(\rho_n+\rho_p)\cdot(\rho_n+\rho_p) - \tfrac{1}{64}(t_1+3t_2)\nabla(\rho_n-\rho_p)\cdot\nabla(\rho_n-\rho_p)$$

where $\langle i|p^2|j\rangle = (-\phi_i^*\nabla^2\phi_j)$

In addition to the density ρ, the Hamiltonian depends on τ, σ, and gradients. We therefore have to define Green's functions for perturbation with any of these operators. Our precise definition is,

$$G^{(0)}_{\alpha\beta}(r_1, r_2) = \sum_{h,p}\left[\frac{\langle h|M_\alpha|p\rangle_{r_1}\ \langle p|M_\beta|h\rangle_{r_2}}{\epsilon_p-\epsilon_h-\omega-i\epsilon} + \frac{\langle p|M_\alpha|h\rangle_{r_1}\ \langle h|M_\beta|p\rangle_{r_2}}{\epsilon_p-\epsilon_h+\omega-i\epsilon}\right] \tag{22}$$

where M_α is one of the operator set $[\sigma, \tau, \nabla, \nabla^2]$ and combinations. Eq. (19) can then be read as a matrix equation in this space of operators.

The RPA interaction can be expressed in terms of the operators $\boldsymbol{\sigma}$ and $\boldsymbol{\tau}$ by the relation

$$\frac{\delta H}{\delta\rho_1\,\delta\rho_2} = \sum_{\sigma,\tau,\sigma',\tau'}\frac{(1+(-1)^{\sigma-\sigma'}\boldsymbol{\sigma}_1\cdot\boldsymbol{\sigma}_2)}{4}\ \frac{(1+(-1)^{\tau-\tau'}\boldsymbol{\tau}_1\cdot\boldsymbol{\tau}_2)}{4}\ \frac{\delta H}{\delta\rho_{\sigma\tau}\,\delta\rho_{\sigma'\tau'}}\,. \tag{23}$$

The gradient operator in a two-body interaction can act on any of four wavefunctions, which we denote by ∇_1, ∇_1', ∇_2, and ∇_2'. The numerical index refers to the two particles. An unprimed gradient acts on the particle coordinate, and a primed gradient acts on the hole coordinate of an ordinary particle–hole scattering. We shall now display the operator expression for the Skyrme interaction, with antisymmetrization implicit. It is

$$\frac{\delta H}{\delta\rho_1\,\delta\rho_2} = \delta(r_{12})[a - b(\nabla_1^2+\nabla_2^2+\nabla_1'^2+\nabla_2'^2+(\nabla_1-\nabla_1')\cdot(\nabla_2-\nabla_2')) + c(\nabla_1+\nabla_1')\cdot(\nabla_2+\nabla_2')] \tag{24}$$

with

$$a = (t_0+\tfrac{1}{2}t_3\rho)(\tfrac{3}{4} - \tfrac{1}{4}\tau_1\cdot\tau_2 - \tfrac{1}{4}\sigma_1\cdot\sigma_2 - \tfrac{1}{4}\sigma_1\cdot\sigma_2\tau_1\cdot\tau_2) + \tfrac{1}{2}t_0x_0(\sigma_1\cdot\sigma_2-\tau_1\cdot\tau_2)\,, \tag{24a}$$

$$b = (\tfrac{3}{32}t_1+\tfrac{5}{32}t_2) + (\tfrac{1}{32}t_2-\tfrac{1}{32}t_1)(\tau_1\cdot\tau_2+\sigma_1\cdot\sigma_2+\tau_1\cdot\tau_2\sigma_1\cdot\sigma_2) \tag{24b}$$

and

$$c = (\tfrac{3}{32}t_1-\tfrac{15}{32}t_2) - (\tfrac{1}{32}t_1+\tfrac{3}{32}t_2)(\tau_1\cdot\tau_2+\sigma_1\cdot\sigma_2+\tau_1\cdot\tau_2\sigma_1\cdot\sigma_2)\,. \tag{24c}$$

All the velocity dependence is in the expression

$$[\nabla_1^2+\nabla_2^2+\nabla_1'^2+\nabla_2'^2+(\nabla_1-\nabla_1')\cdot(\nabla_2-\nabla_2')]\,.$$

This is Galilean-invariant in the particle–hole matrix element

$$\langle \phi_p(1)\phi'_h(2)|V|\phi'_h(1)\phi_n(2)\rangle .$$

4. Algebraic details

We next turn to the question of the numerical representation of $G^{(0)}$ in order to solve eq. (19). We first expand G in spherical harmonics:

$$G(\boldsymbol{r}_1, \boldsymbol{r}_2) = \sum_L G_L(r_1, r_2)\, Y^{L^*}(\hat{\boldsymbol{r}}_1)\cdot Y^L(\hat{\boldsymbol{r}}_2) .$$

Eq. (19) then separates into independent equations for each L. Next we factor $G^{(0)}_{\alpha\beta L}$ as:

$$G^{(0)}_{\alpha\beta L}(r_1, r_2) = \sum_{\text{ph}} C^{\text{ph}L^*}_\alpha(r_1)\, C^{\text{ph}L}_\beta(r_2)\left[\frac{1}{\epsilon_p - \epsilon_h - i\epsilon - \omega} + \frac{\pi_\alpha \pi_\beta}{\epsilon_p - \epsilon_h^- - i\epsilon + \omega}\right] . \tag{25}$$

The sum is over unoccupied orbits p (particle) and occupied orbits h (hole), with the Hartree–Fock energies denoted by ϵ_i. The function C is defined

$$C^{\text{ph}L}_\alpha(r) = \sum_{m_p m_h} \langle j_p m_p j_h - m_h | LM\rangle \langle \phi_p | M_\alpha(r) | \phi_h\rangle (-1)^{j_h - m_h} \tag{26}$$

where ϕ_i is the Hartree–Fock orbital i. Finally, we define π_α as ± 1 according to the parity of M_α under time reversal:

$$\langle h|M_\alpha|p\rangle = \pi_\alpha \langle p|M_\alpha|h\rangle \quad . \tag{27}$$

The parameter π is positive for all common operators except $\boldsymbol{\sigma}$ and $\boldsymbol{p}$.

We shall now find expressions for the C-coefficients. Matrix elements of some of the operators have been given previously [8, 15, 16], but since it is not trivial to calculate all the matrix elements, we shall outline a convenient method. First of all, we express the vector operators in a helicity representation, that is, the operators are in a body coordinate system. Then the two-body δ-interaction is of the form

$$V(\boldsymbol{r}_1, \boldsymbol{r}_2) = \sum_{\alpha, L, M} \frac{\delta(r_1 - r_2)}{r_1 r_2} \frac{2L+1}{4\pi} M^{1^+}_\alpha D^{L^*}_{K_\alpha M}(\hat{\boldsymbol{r}}_1)\cdot D^L_{K_\alpha M}(\hat{\boldsymbol{r}}_2) M^2_\alpha \tag{28}$$

where K_α is the angular momentum of the M_α operator about the $\boldsymbol{r}$ axis. We make a similar expansion for $G_{\alpha\beta}$, with $\sqrt{(2L+1)/4\pi}\, D^L_{K_\alpha M}$ replacing the spherical harmonics. The C-coefficient to be evaluated is then

$$C^{\text{ph}L}_\alpha = \int d\Omega \sqrt{\frac{2L+1}{4\pi}} D^{L^*}_{K_\alpha M}(\Omega) M_\alpha (\phi^{j_p} \phi^{j_h^*})^L_M \quad . \tag{29}$$

From general considerations, the operator product $M_\alpha(\phi^{j_p}\phi^{j_h^*})^L_M$ transforms as a D function, and therefore is proportional to one. The constant of proportionality is obtained by evaluating the product on the z axis:

Table 2
Expressions for C-coefficients according to eq. (31).

Operator	
1	$C_1^{phL}(r) = \phi^{j_p}(r)\,\phi^{j_h}(r)\sqrt{\frac{(j_p+\frac{1}{2})(j_h+\frac{1}{2})}{4\pi(2L+1)}}\,(1+(-)^{l_h+l_p-L})\,(-)^{L+1/2-j_p}(j_p\,\frac{1}{2}\,j_h\,-\frac{1}{2}\,|L0)$
σ_0	same as above except with $(1-(-)^{l_h+l_p-L})$
$\sigma_\pm$	$C_{\sigma_\pm}^{phL}(r) = \phi^{j_p}(r)\,\phi^{j_h}(r)\sqrt{\frac{(j_p+\frac{1}{2})(j_h+\frac{1}{2})}{4\pi(2L+1)}}\cdot(j_p\,\frac{1}{2}\,j_h\,\frac{1}{2}\,|L1)\begin{Bmatrix}(-)^{l_p+l_h-L}\\1\end{Bmatrix}\begin{Bmatrix}\sigma_+\\\sigma_-\end{Bmatrix}$
∇_0^p	$C_{\nabla\theta}^{phL}(r) = C_1^{phL}(r)\,\frac{1}{\phi^{j_p}(r)}\cdot\frac{d\phi^{j_p}(r)}{dr}$
$\nabla_\pm^p$	$C_{\nabla\pm}^{phL}(r) = \frac{\phi^{j_p}(r)\,\phi^{j_h}(r)}{r}\sqrt{\frac{(j_p+\frac{1}{2})(j_h+\frac{1}{2})}{2\cdot4\pi(2L+1)}}\Big\{(j_p\,\frac{3}{2}\,j_h\,-\frac{1}{2}\,|L1)\sqrt{(j_p-\frac{1}{2})(j_p+\frac{3}{2})}$ $-(j_p-\frac{1}{2})(j_p+\frac{3}{2})-(j_p\,\frac{1}{2}\,j_h\,\frac{1}{2}\,|L1)\cdot\begin{Bmatrix}j_p-\frac{1}{2}\\j_p+\frac{3}{2}\end{Bmatrix}(-)^{l_h-j_h+1/2}\,(-)^{l_p-j_p+1/2}\Big\}\begin{Bmatrix}j_p=l_p+\frac{1}{2}\\j_p=l_p-\frac{1}{2}\end{Bmatrix}$

The raising and lowering operators σ_+ and σ_- are defined so that $\sigma\cdot\sigma=\sigma_0\sigma_0+\sigma_+\sigma_-+\sigma_-\sigma_+$ and $\langle\sigma^2\rangle=3$.

$$M_\alpha(r)\,(\phi^{j_p}\phi^{j_h^*})^L_M = D^L_{K_\alpha M}(\hat{r})\,M_\alpha(\hat{z})\,(\phi^{j_p}\phi^{j_h^*})^L_{K_\alpha}\Big|_{\hat{z}}\,. \tag{30}$$

Inserting this in eq. (29) and the well-known orthonormality relations of the D-matrices we find

$$C_\alpha^{phL} = \frac{4\pi}{(2L+1)}\sqrt{\frac{2L+1}{4\pi}}\,M_\alpha(\hat{z})\,(\phi^{j_p}\phi^{j_h^*})^L_{K_\alpha}\Big|_{\hat{z}}\,. \tag{31}$$

At this point, some tedious algebra is necessary to find the value of the operator product on the z-axis. We merely quote the results in table 2. Several different angular momentum coupling coefficients appear, and can all be expressed in terms of the coefficient $(j_p\,\frac{1}{2}\,j_h\,-\frac{1}{2}\,|L0)$ by menas of the reduction formulas

$$(j_1\,\tfrac{1}{2}\,j_2\,\tfrac{1}{2}\,|L1) = \frac{(-1)^{j_1+j_2-L}\,(j_1+\frac{1}{2})\pm(j_2+\frac{1}{2})}{\sqrt{L(L+1)}}\,(j_1\,\tfrac{1}{2}\,j_2\,-\tfrac{1}{2}\,|L0)\,, \tag{32}$$

$$(j_1\,\tfrac{3}{2}\,j_2\,-\tfrac{1}{2}\,|L1) = \frac{\sqrt{L(L+1)}}{\sqrt{(j_1-\frac{1}{2})(j_1+\frac{3}{2})}}\,(j_1\,\tfrac{1}{2}\,j_2\,-\tfrac{1}{2}\,|L0)$$
$$\times\left\{1-\left(\frac{j_2+\frac{1}{2}}{L(L+1)}\right)((-1)^{j_1+j_2-L}\,(j_1+\tfrac{1}{2})+(j_2+\tfrac{1}{2}))\right\}. \tag{33}$$

With this substitution, the formulas for the C-coefficients are in the final form. It is only necessary now to choose a radial mesh, for the equations to be in a form for numerical treatment.

5. General features of the response

Before performing the numerical calculations, it is useful to review the theory of the response function in the limit of infinite matter, although the predictions from this limit do not have a large scope of validity. By translational invariance we need only consider perturbations of the form

$$M_\alpha e^{iq\cdot r} .$$

The bare Green's function is given by the integral

$$G^{(0)}_{\alpha\beta}(q,\omega) = \int \frac{d^3k}{(2\pi)^3}\,\theta(k_F - |k|)\,\theta(|k+q| - k_F)\,\langle k|M_\alpha|k+q\rangle\langle k+q|M_\beta|k\rangle\,\frac{2(\epsilon_{k+q}-\epsilon_k)}{(\epsilon_{k+q}-\epsilon_k)^2 - \omega^2 - i\epsilon} \tag{34}$$

where

$$\left.\begin{aligned}\theta(x) &= 1\\ &= 0\end{aligned}\right\}\begin{cases}x>0\\ x<0\end{cases}$$

and ϵ_k is the Hatree–Fock energy of the k-orbit. With $M_{\alpha,\beta}$ unit operators, the integration can be done analytically to give the Lindhard function [17]. The Landau theory of Fermi liquids is simply the RPA model in the limit that $q/k_F \ll 1$, but with M_α (in principle) an arbitrary function of θ_{kq}. In this limit the free Green's function is

$$G^{(0)}_{ff} \approx \int_{-1}^{+1} \frac{d\cos\theta}{(2\pi)^2}\,\frac{k_F q\cos\theta\, f(\theta)\, f'(\theta)\, n}{(k_F q/m^*)\cos\theta - \omega - i\epsilon} \tag{35}$$

where n is the number of particles in each plane wave state, i.e., 4 for nucleons, and m^* is determined from the Hartree–Fock energies near the Fermi surface. i.e.

$$\epsilon_p \sim \frac{p^2}{2m^*} + \epsilon_0 \quad \text{with} \quad p \approx k_F . \tag{36}$$

To get the static response, we need the $\omega = 0$ limit of the above Green's function. Let us also confine ourselves to the unit operator. Then we have

$$G^{(0)}_{11}(q,0) = n\,2k_F m^*/(2\pi)^2 . \tag{37}$$

The scalar static response is proportional to the RPA Green's function, which in this case is

$$G^{RPA}(0) = \frac{G^{(0)}_{11}}{(1 + (\delta V/\delta\rho)\, n k_F m^*/2\pi^2)} = \frac{1}{(1+F_0)}\,G^{(0)}_{11} . \tag{38}$$

In the last expression we use the traditional dimensionless expression,

$$F_0 = \frac{\delta V}{\delta\rho}\,\frac{n k_F m^*}{2\pi^2} . \tag{39}$$

If F_0 is positive, coming from a repulsive interaction, the response is less than in a free Fermi gas. If F_0 is less than -1, the Hartree–Fock ground state is unstable.

To find the eigenfrequencies of the system, we need the poles of $G^{\mathrm{RPA}}(\omega)$. The first thing to be noted is that attractive and repulsive interactions have different behavior. For a repulsive interaction, a solution will be found for ω real and greater than $k_{\mathrm{F}}q/m^*$. Attractive interactions yield solutions with ω complex. The strength is broadly distributed from 0 to $\omega = k_{\mathrm{F}}q/m^*$, the so-called Landau damping of the excitation. For the repulsive interactions, we can make a simple estimate of the energies of the poles assuming $k_{\mathrm{F}}q/m^* \ll \omega$. Then expanding the bare Green's function for the unit operator, we have

$$G_{11}^{(0)}(q, \omega) \sim \frac{-nk_{\mathrm{F}}^3 q^2}{\omega^2 m^* 6\pi^2} .$$

The poles of G^{RPA} are given by

$$\omega^2 = n \frac{\delta V}{\delta \rho} \frac{k_{\mathrm{F}}^3 q^2}{m^* 6\pi^2} \approx \frac{F_0}{3} \left(\frac{k_{\mathrm{F}} q}{m^*}\right)^2 . \tag{40}$$

The point we wish to abstract from this formula, which remains valid in less crude models, is that the eigenenergy is proportional to the single-particle excitation energy, with the proportionality constant dependent on the strength of the interaction. For later use we shall rewrite eq. (40) in the form

$$\omega_q \sim \sqrt{\frac{2F_0}{3} \frac{m}{m^*}}\, \bar{\omega}_q \tag{41}$$

where $\bar{\omega}$ is the average energy of an excitation in the noninteracting system. Naturally, we can define response functions for nonscalar operators such as σ and τ. These operators do not couple to each other or to the scalar operators if the ground state has $S = 0$ and $T = 0$.

Further consideration of the response depends on the properties of the interaction. Of the interactions which give realistic Hartree–Fock theories, we shall deal with Skyrme I (SkI) and Skyrme II (SkII) of ref. [9]. Interactions I and II represent extremes in the range of behavior that a realistic interaction could have and still achieve saturation at the right energy and density. Interaction I has an extreme of density dependence, while interaction II has a milder density dependence but a strong velocity dependence. The derived Skyrme interaction (NV) of Negele and Vautherin [11] has a density dependence close to SkI, but also a strong velocity dependence. We can characterize the velocity dependence by the predicted effective mass m^* in Hartree–Fock theory. This is given by

$$\frac{1}{m^*} = \frac{1}{m} (1 + B(\rho))$$

and the effective masses of SkI, II and NV are given in table 3. Experimental evidence for the true m^*/m is ambiguous, but see for example refs. [18, 19].

We next consider the interaction strengths in the infinite medium. We substitute k_{F} for p in eq. (21), and determine the various spin–isospin contributions with eq. (23). The results for the dimensionless interaction strength calculated at $\rho = 0.16$ fm^{-3} are given in table 4. We note that for SkI, the σ interaction is too attractive for stability. This has emerged in a calculation of ^{16}O

Table 3
Effective masses.

Interaction	m^*/m
SkI	0.91
SkII	0.56
NV	0.63

Table 4
Interaction strengths in nuclear matter ($\rho = 0.16$ fm^{-3}). The dimensionless F parameters are related to the interaction energies by eqs. (23) and (39).

Interaction	SkI	SkII	NV	Bäckman [21]	Speth [22]
F_1	0.7	−0.1	−0.3	−0.6	−0.2
F_τ	1.2	0.5	2.2	0.3	1.7
F_σ	−2.3	−0.7	–	0.6	1.4
$F_{\sigma\tau}$	−0.6	−0.1	–	0.4	1.8

spectra, where the 2^- state came out below the ground state [20]. We believe that this instability may be traced to the specific parametrization of the density dependence of the interaction, that 3 particles at the same point have an effective repulsion. Since 3 particles can only come to the same point with the spins partially paired, the three-body term is an effective depairing interaction. Possibly a deeper consideration of the origin of the three-body repulsion would show some of the effect due to the Pauli principle operative between particles in $S = 1$ states, in which case F_σ would not be so attractive.

In any case, since SkI and SkII are fitted to ground state properties of even–even nuclei, assuming the spins paired, there is no reason to expect the spin-dependence part of the interaction to be realistic. The scalar part should be reliable, since basically scalar properties are fit, and the isovector part should also be reasonable, since the fit includes a variety of nuclei with differing isospin. The third column of the table shows the interaction parameters derived from the Hamiltonian density of Negele and Vautherin [11], their table 1. The interaction is obtained explicitly from the second derivative of the Hamiltonian density, eq. (23). Since these authors consider only the spin-independent Hamiltonian density, we do not attempt to extract a spin-dependent interaction. Also shown in table 4 is the prediction by Bäckman [21], who used a simplified realistic interaction to derive his parameters. His notation differs from ours; his F_0, F_0', G_0, G_0' means $F_1, F_\tau, F_\sigma, F_{\sigma\tau}$, respectively. In the last column are the parameters derived from a phenomenological RPA model of Ring and Speth [22]. The density dependent interaction in this model was chosen to fit the energy and lifetime of the lowest 3^- and 2^+ states in ^{208}Pb, as well as moments in neighboring nuclei.

Unfortunately, the low energy response of the nucleus is dominated by the surface region, for which the infinite matter results of the preceding paragraphs are not at all reliable. To begin to make a theory which includes the surface, we need some knowledge of the spacial dependence of the low-frequency transition densities. These transition densities could be constructed with the help of a classical ansatz, as was first done by Tassie [23], or from a variational principle [24]. The Tassie model predicts an approximate Green's function of the form

Table 5
Interaction strengths, eq. (39), at half nuclear matter density ($\rho = 0.08\ \mathrm{fm}^{-3}$).

Interaction	SkI	SkII	NV	Bäckman	Speth
F_1	−1.6	−1.0	−2.7	−1.1	−2.0
F_τ	1.7	0.9	2.1	0.6	0.7
F_σ	−1.0	−0.2	–	0.4	–
$F_{\sigma\tau}$	0.3	0.3	–	0.5	–

$$G_L(r, r', \omega) \sim \frac{\chi^L(r)\chi^L(r')}{\omega_0^2 - \omega^2}\ , \tag{42}$$

where

$$\chi^L(r) \sim r^{L-1}\ \mathrm{d}\rho/\mathrm{d}r\ , \qquad L \neq 0 \tag{43a}$$

$$3\rho + r\ \mathrm{d}\rho/\mathrm{d}r\ , \qquad L = 0 \tag{43b}$$

and ω_0 is unspecified by the theory. It may be seen that, except for $L = 0$, the perturbation is confined to the surface of the nucleus. Remarkably, this model can be derived [25–27] from sum rules under the assumption that the strength of a probing field $r^L Y^L M_\alpha$ is exhausted by a single resonance. This assumption is reasonable for the operators with repulsive F's, since in the limit of the Landau theory, a single collective mode dominates the strength function. The assumption is difficult to justify for attractive interactions, in view of the Landau damping. Nevertheless, empirically the model is quite successful for the scalar resonances, where the empirical interaction is attractive. Since the surface region is so important, the interaction strength should be examined here as well. In the surface region, the interaction is quite different from the interior. In table 5, the F parameters are evaluated at the surface density of $0.08\ \mathrm{fm}^{-3}$. We see now that F_1 is strongly attractive. This corresponds more closely than the previous numbers to the properties of the empirical or calculated response function.

6. Sum rules

From general principles, the strength function satisfies an energy-weighted sum rule,

$$\sum_n (E_n - E_0)|\langle n|F|0\rangle|^2 = \tfrac{1}{2}\langle|[F, [H, F]]|\rangle\ . \tag{44}$$

This sum rule is automatically satisfied in RPA, if the left-hand side is evaluated by eq. (3b) and the right-hand side is evaluated by taking the expectation of the double commutator in the Hartree–Fock ground state. This theorem was proved by Thouless [6] using configuration space representation of the wavefunctions. The theorem can be proved quite easily in the Green's function formalism [71], as we shall now show. It is only necessary to consider the first two terms in the series expansion of G^{RPA}

$$G^{\mathrm{RPA}} = G^{(0)} - G^{(0)} \frac{\delta H}{\delta \rho} G^{(0)} + \dots . \tag{45}$$

It will be seen below that the higher order terms do not contribute to the energy-weighted strength. It will also be necessary to express the Hamiltonian in a Hartree–Fock basis. We can write

$$H = H_{\mathrm{HF}} + H_{\mathrm{V}} ,$$

where H_{HF} has off-diagonal matrix elements for at most one particle, and H_{V} has only off-diagonal matrix element for two particles. Terms in the Hamiltonian off-diagonal in more than two particles play no role.

We now evaluate the sum rule with (45). The first term makes a contribution

$$\frac{1}{\pi} \mathrm{Im} \int_0^{\infty} \mathrm{d}\omega\, \omega \sum_{\mathrm{h,p}} |\langle \mathrm{h}|F|\mathrm{p}\rangle|^2 \left(\frac{1}{\epsilon_{\mathrm{p}} - \epsilon_{\mathrm{h}} - \omega - \mathrm{i}\epsilon} + \frac{1}{\epsilon_{\mathrm{p}} - \epsilon_{\mathrm{h}} + \omega - \mathrm{i}\epsilon} \right)$$

$$= \frac{1}{\pi} \mathrm{Im} \int_{-\infty}^{+\infty} \mathrm{d}\omega\, \omega \sum_{\mathrm{h,p}} |\langle \mathrm{h}|F|\mathrm{p}\rangle|^2 \frac{1}{\epsilon_{\mathrm{p}} - \epsilon_{\mathrm{h}} - \omega - \mathrm{i}\epsilon} = \sum_{\mathrm{ph}} |\langle \mathrm{h}|F|\mathrm{p}\rangle|^2 (\epsilon_{\mathrm{p}} - \epsilon_{\mathrm{h}}) . \tag{46}$$

The sum is restricted to occupied orbits on the h index and unoccupied orbits on the p index. However, there is no need to restrict the p sum, because a term with $(\epsilon_{\mathrm{h}'} - \epsilon_{\mathrm{h}})$ is cancelled by a similar term with $(\epsilon_{\mathrm{h}} - \epsilon_{\mathrm{h}'})$. Thus we can use closure on the p sum to get

$$\int_0^{\infty} \mathrm{d}\omega\, \omega \frac{1}{\pi} \mathrm{Im} \langle F G^{(0)} F\rangle = \tfrac{1}{2} \sum_{\mathrm{h}} \langle \mathrm{h}|[F,[H_{\mathrm{HF}}, F]]|\mathrm{h}\rangle . \tag{47}$$

The second term in the expansion of G^{RPA} can be written

$$\mathrm{Im} \frac{1}{\pi} \int_0^{\infty} \mathrm{d}\omega\, \omega \langle F G^{(0)} V G^{(0)} F\rangle$$

$$= \mathrm{Im} \frac{1}{\pi} \int_{-\infty}^{+\infty} \mathrm{d}\omega\, \omega \sum_{\substack{\mathrm{ph} \\ \mathrm{p'h'}}} \langle \mathrm{h}|F|\mathrm{p}\rangle \frac{1}{\epsilon_{\mathrm{p}} - \epsilon_{\mathrm{h}} - \omega - \mathrm{i}\epsilon} \left\{ \langle \mathrm{ph}|V|\mathrm{p'h'}\rangle \frac{1}{\epsilon_{\mathrm{p'}} - \epsilon_{\mathrm{h'}} - \omega - \mathrm{i}\epsilon} \langle \mathrm{p'}|F|\mathrm{h'}\rangle \right.$$

$$\left. + \langle \mathrm{ph}|V|\mathrm{h'p'}\rangle \frac{1}{\epsilon_{\mathrm{p'}} - \epsilon_{\mathrm{h'}} + \omega - \mathrm{i}\epsilon} \langle \mathrm{h'}|F|\mathrm{p'}\rangle \right\}$$

$$= \sum_{\substack{\mathrm{ph} \\ \mathrm{p'h'}}} \langle \mathrm{h}|F|\mathrm{p}\rangle \{ \langle \mathrm{ph}|V|\mathrm{p'h'}\rangle \langle \mathrm{p'}|F|\mathrm{h'}\rangle + \langle \mathrm{h'}|F|\mathrm{p'}\rangle \langle \mathrm{ph}|V|\mathrm{h'p'}\rangle \} . \tag{48}$$

Again, we need not restrict the p orbits to the unoccupied orbits. This allows us to replace the sum over p and p' by the unit operator, and we end up with the double commutator of H_{V}. The contour integral over higher terms in the Green's function expansion vanish, because the integrands vary as $1/\omega^2$ or faster, and we can close the contour on a pole-free half plane. So our final result is

$$\int_0^\infty d\omega\, \omega \frac{1}{\pi} \mathrm{Im} \langle F G^{\mathrm{RPA}} F \rangle = \tfrac{1}{2} \langle | [F, [H_{\mathrm{HF}} + H_{\mathrm{V}}, F]] | \rangle . \tag{49}$$

The free Green's function satisfies the sum rule with H_{HF}, and the first two terms in the expansion satisfy the complete sum rule. Higher terms merely readjust the strength, preserving the sum rule. In simpler models where H_{V} is invariant under interchange of particles and holes, the second term has no effect on the sum rule.

The sum rule provides a convenient way to show that a spurious state is degenerate with the ground state. We consider the operator $F = \nabla$, which commutes with any Galilean-invariant Hamiltonian. The right-hand side of the sum rule is zero; the only way this can be satisfied is for all of the strength to be exhausted by a state at zero energy.

Let us now examine what the Skyrme Hamiltonians predict for sum rules. The single-particle kinetic energy gives the following contribution to sum rules [12]:

$$\sum_n |\langle 0| \sum r^L Y^L |n\rangle|^2 (E_n - E_0) = \frac{\hbar^2}{8\pi m} AL(2L+1) \langle r^{2L-2} \rangle . \tag{50}$$

The double commutator of the Skyrme interaction vanishes because of the zero range of the interaction, except of operators F carrying spin or isospin. As indicated earlier, the spin-dependent Skyrme interaction is completely unrealistic, so it is only useful to evaluate the isospin sum rules.

In the sum rule for the electric dipole state, the operator is to act only on the protons. With a proper account of the center-of-mass coordinate, the dipole operator should be

$$F_1 = \sum_{\mathrm{p}} \frac{N}{A} r_{\mathrm{p}} Y^1(r_{\mathrm{p}}) - \sum_{\mathrm{n}} \frac{Z}{A} r_{\mathrm{n}} Y^1(r_{\mathrm{n}})$$

which results in the factor A being replaced by NZ/A in eq. (50). Using the same operator, the double commutator of the Skyrme interaction reduces to

$$\tfrac{1}{2} \langle 0 | [F_1, [V_{\mathrm{Skyrme}}, F_1]] | 0 \rangle = \left(\frac{t_1 + t_2}{4} \right) \frac{NZ}{A^2} \frac{3}{4\pi} \left\langle \sum_{ij} \delta(r_{ij}) \right\rangle . \tag{51}$$

This potential contribution to the sum rule is commonly expressed as a fraction α of the kinetic sum rule,

$$\alpha = \frac{\frac{1}{4}(t_1 + t_2) \langle \Sigma_{ij} \delta(r_{ij}) \rangle}{(\hbar^2/2m) A} \tag{52}$$

so that the dipole sum rule becomes

$$\sum_{\mathrm{n}} |\langle 0 | F_1 | \mathrm{n} \rangle|^2 (E_{\mathrm{n}} - E_0) = \frac{\hbar^2}{2m} \frac{3}{4\pi} \frac{NZ}{A} (1 + \alpha) . \tag{53}$$

It is interesting to see how the combination $(t_1 + t_2)$ in eq. (51) emerges from the Hartree–Fock and RPA Hamiltonians. The Hartree–Fock field contains a velocity-dependent term proportional to $(3t_1 + 5t_2)/16$, as may be seen from eq. (21) and table 1. This term primarily modifies the single-particle energies, and affects the sum rule by changing the position of the state. The residual isovector interaction, eq. (24), contains a current–current term proportional to $(t_1 - t_2)/16$,

Table 6
Interaction energy corrections to dipole sum rule, eq. (52). Numbers in parentheses are obtained by numerically integrating the calculated response.

Nucleus	SkI	SkII
^{16}O	0.16 (0.10)	0.57 (0.35)
^{40}Ca	0.19 (0.19)	0.71 (0.70)
^{90}Zr	0.20 (0.18)	0.73 (0.66)
^{208}Pb	0.21 (0.26)	0.79 (0.73)

which affects the strength of the state as much as its position. The sum of these two in eq. (48) is $\frac{1}{4}(t_1 + t_2)$, which is the desired combination.

Experimentally, the dipole sum rule is not unequivocably determined. We have to cut off the sum at some energy. A natural cutoff is the meson production threshold, at which the sum rule is 1.5–2 times the free value [28]. If the cutoff is some energy just above the gaint dipole resonance, the sum rule ranges from 0.6 in ^{16}O to 1.15 ± 0.08 in ^{208}Pb (refs. [29–30]). We believe this is the appropriate cutoff for Hartree–Fock models, for the following reason. The model used a limited configuration space, so it cannot include explicit effects of the meson degrees of freedom or the short range tensor interaction. Therefore, the predictions for the dipole absorption should be just missing the parts due to these aspects of the wavefunction. The tensor interaction has been shown to increase [31] the sum rule from 1.4 to as much as 2.0; the states responsible for this increase would be mostly 2p 2h in our representation and not accessible with our model even if a tensor interaction were included.

The calculated values of α with eq. (52) are given in table 6. There is a great difference between SkI and SkII. SkII predicts a large enhancement, $\alpha \sim 0.7$, which can be traced to the larger particle–hole energies. Comparing the Skyrme models with the empirical sum rule, we see that SkII has too much velocity dependence, and SkI has a much more reasonable velocity dependence. We shall find that neither interaction gives a good account of the isovector properties of nuclei.

7. Numerical details

The first ingredient in an RPA calculation is the complete Hartree–Fock theory of the ground state, i.e. the single-particle wavefunctions and energies. Initially we used Woods–Saxon wavefunctions [32], but we have since constructed a Hartree–Fock program for this purpose. The continuum is handled by putting the nucleus in a box whose radius is several fermis greater than the nuclear radius. Some details which we felt were unimportant were left out. This includes the effect of the spin–orbit potential on the wavefunctions, and Coulomb effects, except as noted later. Our energies correspond to within an MeV of the energies of ref. [9], except for ^{208}Pb, where our levels are more bound by about 5 MeV. The radii are identical to those of ref. [9].

A very strong test of the technique is the calculation of the $J = 1$, $T = 0$ response, which is governed by the spurious state. In a self-consistent RPA calculation, the state must occur at $\omega = 0$. For density-dependent interactions we find that self-consistency can be achieved only when a very large space is included in the bare Green's function. Of course, the interaction can

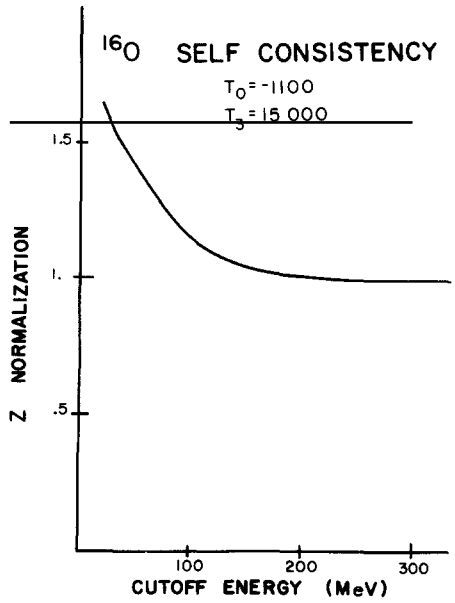

Fig. 1. Self-consistency of spurious state in ^{16}O. The interaction renormalization Z of the Skyrme interaction $t_0 = -1100$ MeV fm^3, $t_3 = 15000$ MeV fm^6, required to produce the spurious state at zero energy is plotted as a function of the cutoff energy in the particle–hole space included in $G^{(0)}$.

always be adjusted to put the spurious state at zero energy, as was done in ref. [32]. For the detailed calculations here, we shall also be content to use a relatively small space. To make up for the inadequacy of $G^{(0)}$, the interaction is adjusted by an overall scaling factor Z which puts the spurious state at zero energy. The convergence of Z to 1 as the space gets large is illustrated in fig. 1. Here is plotted the renormalization factor Z against the maximum particle–hole energy for configurations to be included in $G^{(0)}$. Evidently self-consistency is not achieved until 200 MeV. The cause for this unexpected result lies in the nature of the interaction. The interaction changes very sharply from the surface region to the interior, as it must to give saturation. The space of wavefunctions has to be large enough to include such wavelength changes, to make a self-consistent density perturbation. The wavelength is of order of the surface thickness, which implies an energy of the same order as we actually needed.

We still have to decide how many operators to include in the Green's function and the mesh size in coordinate space. The operator sets which we used are given in table 7. Operator set A has the full velocity dependence of the interaction but neglects the spin and isospin degrees of freedom. It is appropriate for scalar perturbations. The set A_τ is similar to set A except that it is for isovector probes. For $T = 0$ nuclei, the Green's function does not mix these operator sets. The set B has the full spin-isospin degrees of freedom but neglects the velocity dependence of the interaction, and so is exact only for interactions without velocity dependence, such as the one in ref. [10]. The usefulness of this operator set is mitigated by the known incorrect behavior of the $\sigma \cdot \sigma$ interaction. It would probably be better to ignore the $\sigma \cdot \sigma$ interaction than include according to the interactions SkI or SkII. Finally, the operator set C is useful for the electromagnetic response in nuclei with $T \neq 0$. Programs for each operator set consist of about 300

Table 7
Operator sets for response function.

A, A_τ	$(1+\nabla^2), p_\pm, p_r, \nabla_r, \nabla_\pm$	$\times 1$, $\times \tau_z$
B	$1, \tau_z, \sigma, \sigma\cdot\tau$	
C	$\frac{1}{2}(1+\tau_z), \frac{1}{2}(1-\tau_z)$	

Table 8
Numerical approximations in response function calculation.

Nucleus	Mesh size ΔR (fm)	E_{max} (MeV)	Number of particle orbits	Z_{SkI}	Z_{SkII}	Highest number of configuration calculated	Multipolarity with highest number of configurations
^{16}O	0.625	100	30	1.005	0.899	54	2
^{40}Ca	0.625	100	40	1.078	1.001	98	3
^{90}Zr	0.90	40	40	1.114	0.965	114	3
^{208}Pb	1.0	40	50	1.09	0.955	226	4

The number of unoccupied particle orbits and number of configurations contributing to $G^{(0)}$ is determined by the size of the coordinate-space box in which the nucleus is placed, and the energy cutoff, $\epsilon_p - \epsilon_h \leqslant E_{max}$. Z is the renormalization factor needed to achieve self-consistency.

Fortran cards apiece, and are available upon request from the authors. Our Hartree–Fock program is also available.

The size of the configuration space and the mesh size in coordinate space are governed by the limitations of our computer. For most of the calculations, we used a mesh size of 1.0 fm, which tests on finer meshes showed to be accurate to about 5%. We are also forced to truncate the sum for $G^{(0)}$ by only including particle–hole configurations up to a certain energy, E_{max}. The specific energy truncation and mesh sizes are given in table 8, together with the number of single-particle orbitals and particle–hole configurations needed in $G^{(0)}$ with this truncation. The renormalization factors Z, which are included in the calculation of all multipoles, are listed for both SkI and SkII. For the calculations of the strength function in the following section, we computed Im G in steps of 1 MeV, averaging over an interval of 1 MeV by adding a finite imaginary part to ω. Thus, individual resonances will have a width of 1 MeV due solely to the averaging. Computation of G^L at one energy requires $\frac{1}{4}$ minute with set C and 5 minutes with set A. Operator set A is the most realistic; in ref. [32] there was a further truncation in the neglect of ∇_r and p_r, which modifies some of the preliminary conclusions given there.

8. Distribution of strength

We now display the computed strength functions for the various multipoles, eq. (3b). Before examining each multipole in turn, we note some general features which are well-known from the

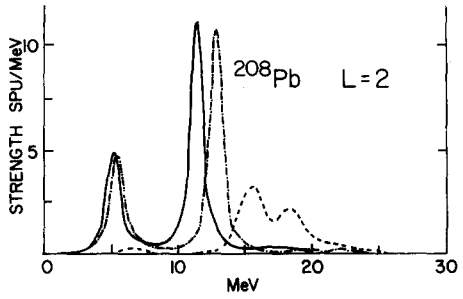

Fig. 2. Isoscalar quadrupole strength in ^{208}Pb, $2 \rightarrow 0$, plotted in Weisskopf units/MeV (eq. (57)). The dashed curve is with a SkI Hartree–Fock Hamiltonian but no interactions between the particles, i.e. $G^{(0)}$. The solid curve is the prediction with the SkI interaction turned on, and the dot-dashed curve is the corresponding full model with SkII.

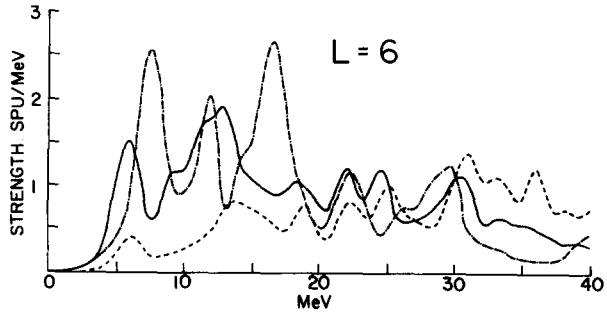

Fig. 3. $L = 6$ strength in ^{208}Pb, $6 \rightarrow 0$, plotted in Weisskopf units/MeV. As before, the dashed curve is the noninteraction SkI model, and the solid and dot-dash curves are the complete SkI and SkII models.

behavior of more schematic models, and also emerge from our calculations. The attractive isoscalar interaction caused the strength to be much enhanced for the lower energies, when compared to the $G^{(0)}$ strength. Furthermore, for the low multipoles, the strength tends to be concentrated in a single state. This is illustrated in fig. 2 for the quadrupole response of ^{208}Pb. The dashed curve is the unperturbed response $G^{(0)}$, for SkI; the solid curve is with SkI interaction; and the dot-dashed curve is with SkII. These strength functions are curves rather than sets of δ-function spikes because of the averaging in the calculation of Im G. Note that the interaction shifts the bulk of the strength downward and also makes it narrower. Since the energy-weighted sum rule is conserved, the downward shift in strength is accompanied by an increase in magnitude. We also see that there is a considerable difference between SkI and SkII, with SkI predicting a lower resonance energy.

It is interesting also to examine how high in multipolarity and energy the Green's function must be taken for the strength function to approach that of the noninteracting system. For L higher than 3, the strength does not concentrate in a single giant resonance, but up to $L = 6$ it remains quite different from the free response. The $L = 6$ response in ^{208}Pb in fig. 3 illustrates the approach to the noninteracting limit. The dashed (noninteracting) and solid (SkI) curves are quite close above 15 MeV. Below 10 MeV, however, there is still pronounced collectivity.

We now take up in detail the strength functions of the important lower multipolarities. Except for the monopole and isovector strengths, the SkI results below are very similar to the recent results of Ring and Speth [22], who use an oscillator basis, a Woods–Saxon single-particle Hamiltonian, and a phenomenological density-dependent two-particle interaction.

Isoscalar monopole ($L = 0$, $T = 0$). This multipole is the breathing mode which has been the subject of several calculations [34–36]. This mode is important in determining two experimental properties, namely isotope shifts [37] and the mass dependence of particle transfer form factors. From fig. 4, a plot of the strength versus energy in ^{208}Pb, we first note that the single-particle energy is quite a bit higher than the traditional $2\hbar\omega$ value, even with the SkI interaction, which is nearly velocity independent. This is due to the fact that in a realistic well it is relatively more costly to make a radial node than angular node. We also see from the figure that with the interaction turned on, the mode is shifted slightly down in energy. Ring and Speth [22] find the

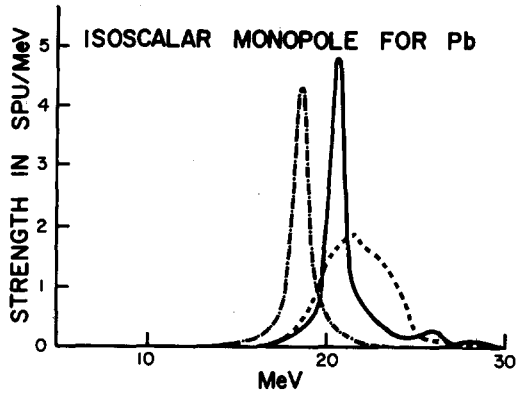

Fig. 4. Strength of the monopole operator, $\Sigma_i r_i^2$, in ^{208}Pb. As before, the dashed curve is the SkI Hartree–Fock model with no residual interaction, and the solid and dot-dashed curves are the complete SkI and SkII models.

monopole concentrated at 14 MeV in ^{208}Pb, much lower than our 18 MeV. Referring to table 4, it may be seen that these authors have a more attractive interaction in the infinite matter limit, so it is not surprising that their monopole is lower. One should be cautious in using these infinite matter Landau parameters however. The downward shift of the strength with the SkI interaction is contrary to what would be anticipated from the repulsive Landau parameter F_0. We will return later to the systematics of the resonance energy as a function of nuclear mass.

Isoscalar quadrupole ($L = 2$, $T = 0$). Giant quadrupole strengths have recently been seen as fairly sharp peaks in inelastic scattering [38–41]. As may be seen from fig. 5 of the SkI systematics, we also find that there is a sharp state. A giant resonance at this energy was predicted by Mottelson [42] using the harmonic oscillator model. We shall examine the A-dependence of the

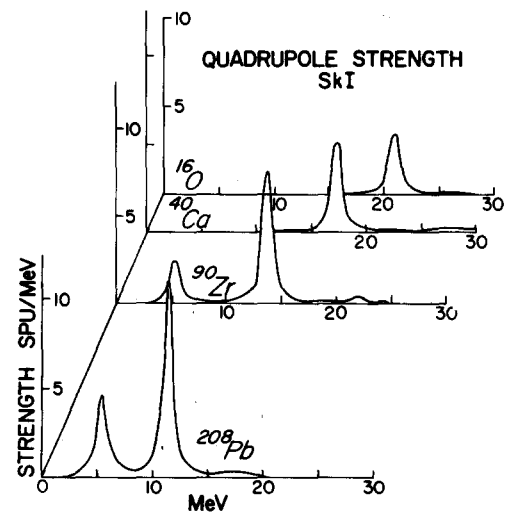

Fig. 5. Systematics of the quadrupole strength in various closed shell nuclei. The Hamiltonian is SkI, the averaging interval is 1 MeV, and the mesh size is 1 MeV.

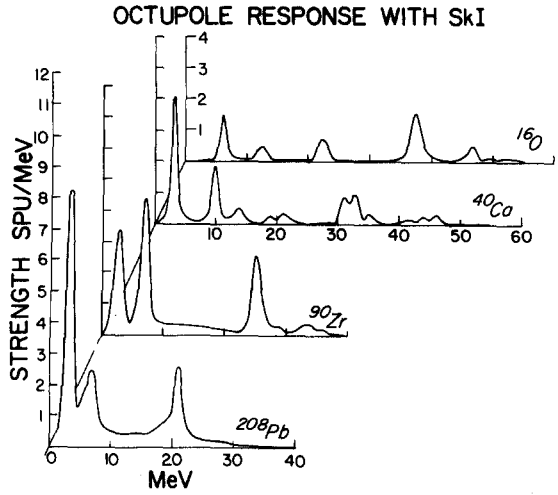

Fig. 6. Systematics of the octupole strength with the SkI Hamiltonian.

energetics in a later section; SkI and SkII are systematically different with SkI in agreement with experiment.

One feature of the calculated response that may seem surprising is that the upper state is sharp. According to the Landau theory, the strength should be rather spread out, since the interaction is attractive. However, this is only a consequence of $G^{(0)}$ having a significant strength throughout the energy region of interest. From fig. 2 we see that the $G^{(0)}$ strength is lumped above 14 MeV in ^{208}Pb. Indeed, the tiny piece of it below 10 MeV generates a low state having nearly 30% of the main peak. Another point of interest to the authors is that there is no evidence for the separation of the vibration into a surface mode and a distinct volume mode, as might be expected of a moderately compressible fluid. In fact, the fluid picture is quite wrong for the giant modes [24], and even predicts the wrong A-dependence for the energy.

Isoscalar octupole ($L = 3$, $T = 0$). The general features of the octupole strength function undergo a smooth change from light to heavy nuclei. Fig. 6, of the SkI octupole systematics, shows that for light nuclei the strength function is spread out over many energy regions, while as we progress to heavier nuclei the lowest state collects more and more strength. It seems plausible, although we cannot prove it, that a high-angular momentum multipole, such as 3^-, would require a large nucleus to have its collective properties fully exhibited. The very large peak in ^{208}Pb is somewhat deceptive; actually the state contains only 17% of the (isoscalar) energy-weighted sum rule. Details on the comparison of strengths with experiment we defer to a following section.

Another point of interest in the octupole strength function is comparison with the harmonic oscillator model. In this model, the strength is split into two peaks, at $\hbar\omega$ and at $3\hbar\omega$, with the bulk of the strength in the $3\hbar\omega$ peak. From fig. 6, it appears that the $3\hbar\omega$ strength is still large and sharp in ^{16}O. This upper state actually becomes quite broad when the box is chosen with a larger radius*. In heavier nuclei, the $3\hbar\omega$ strength becomes progressively weaker. The upper part

* We are indebted to S. Shlomo for calculations on this point.

of the 3^- strength in ^{208}Pb has reportedly been observed in electron scattering [40].

Isovector dipole ($L = 1$, $T = 1$). The fundamental giant dipole resonance has been the object of theoretical study ever since its discovery in 1948. Since the nature of the resonance as a many-body phenomenon is now well understood, the main question is whether its position and fragmentation is consistent with the known properties of the nuclear interaction. The answer to this is ambiguous; microscopic calculations [43] have had difficulty reproducing the energy of the state in ^{208}Pb. On the other hand, macroscopic calculations [42] based on the empirical isovector optical potential do quite well on the mean energy of the strength. Our calculations with the Sk interactions should be in this latter category, since the interactions are fitted to isovector as well as isoscalar ground state properties. The results of our calculations are exhibited in figs. 7 and 8 In fig. 7, the unperturbed SkI strength in ^{208}Pb is compared with the interacting SkI and SkII response. The SkII interaction has a much higher energy-weighted strength than SkI. Also, the strength function is split into two peaks for both interactions. In actuality, only one peak is observed [29], located at 13.5 MeV, and it has a strength less than the total of both SkI peaks.

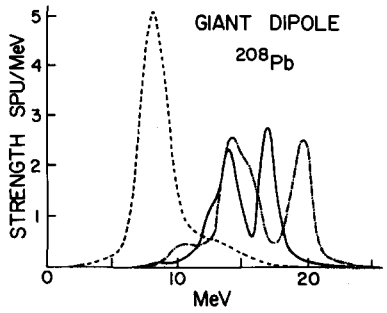

Fig. 7. Giant dipole strenght in ^{208}Pb. Solid curve is SkI, dot-dashed is SkII, and dashed curve is SkI without a residual interaction. Note that the integrated strength for SkII is larger than for SkI.

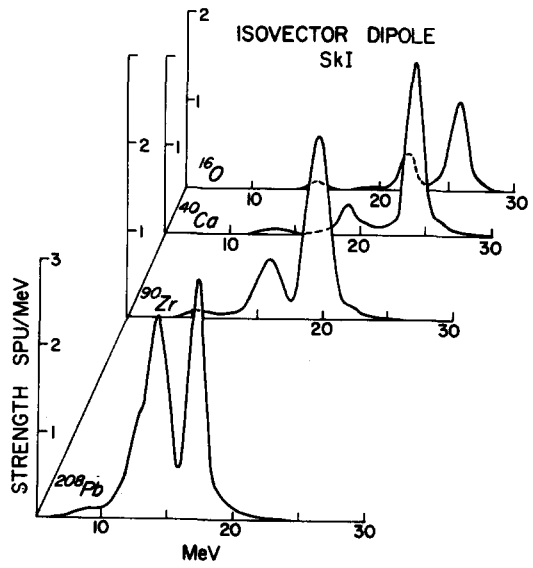

Fig. 8. Systematics of the giant dipole for the SkI Hamiltonian.

There is no evidence for additional strength at higher energy. Thus the models fail to give a quantitative account of the dipole.

Turning to fig. 8, the systematics of the strength function in different nuclei, we see that the splitting of the dipole into two pieces is quite a general phenomenon. This splitting was noted in the pioneering calculations [44, 45] on ^{16}O; there it originates in the single-particle spin–orbit potential.

The origin of the theoretical split into two peaks for heavier nuclei is not clear. The velocity-dependence of the interaction plays some role in this effect; when this part of the interaction is turned off the upper peak becomes much smaller. Other calculations with velocity-independent interactions [48–49] or realistic interactions [43] have also found a small peak at higher excitation.

In ^{16}O, there are in fact two prominent peaks at 22 and 24 MeV, and extending upward to 30 MeV there is a broad absorption. The SkII prediction for ^{16}O, not graphed, is excessively high, but our SkI prediction has at least a reasonable lower peak.

Since neither SkI nor SkII gives a good description of the dipole, it is appropriate to ask in what way do they err. We find that a reasonable model can be constructed with SkI, but omitting the velocity-dependent $p_i p_j$ terms in the residual interaction, i.e. operator set C.

It should be emphasized again that the basic question of the broadening of peaks is outside the scope of our model; the apparent widths in the figures tend to be numerical artifacts. The physical origin of the widths, at least in heavy nuclei, is the mixing with more complicated states [50–52].

Isovector monopole and quadrupole. Other isovector modes which have attracted some interest are the monopole and the quadrupole. The isovector monopole influences isospin violating effects, because it couples strongly to the Coulomb field. It has been invoked in the theory of superallowed beta decay [53], the theory of widths of analog states [54–55], and the Coulomb energies of mirror nuclei [26]. The isovector monopole only enters these problems as a virtual state, so it is only the mean energy of the strength that is of interest. We shall explore this further below.

Recently E1–E2 interference has been observed above the giant dipole resonance, in the nuclei ^{16}O (ref. [56]) and ^{208}Pb (ref. [57]). The claim was made that the E2 is from a giant isovector quadrupole. The theoretical predictions for this mode is not likely to be meaningful with the full SkI or SkII interactions, so we only mention the predictions with the operator set C. We find that in ^{16}O the giant quadrupole has only 20% of the sum rule below 30 MeV, where the interference of ref. [56] was observed. In ^{208}Pb however, we find a concentration of strength between 20 and 22 MeV, which compares well with the observed strength seen in electron scattering [40], which is centered at 22 MeV. The gamma experiments [57] places the strength somewhat higher, at 23.7 MeV.

9. Transition densities

One of the features of most multipoles is the existence of single states carrying much of the transition strength. What do these sharp states look like? The transition densities to individual states can be computed by examining the Green's function near a pole, where it reduces to a dyadic operator, as in eq. (42). The collective model, specified by eq. (43), has been shown to work quite well empirically for the transition densities for the strong isoscalar states [29]. We find that both Skyrme I and II predict isoscalar transition densities very close to the collective model [33]. An

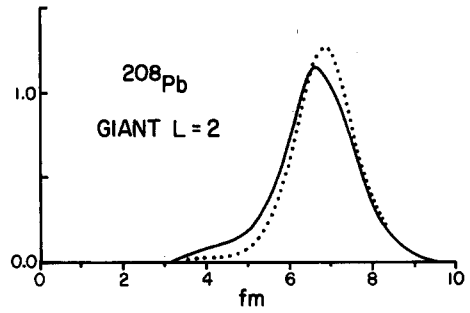

Fig. 9. Isoscalar quadrupole transition density ($\times r^2$) in ^{208}Pb with the SkI interaction to the giant state predicted at 11.4 MeV. The solid curve is the calculation; the dashed curve is the collective model, eq. (43a).

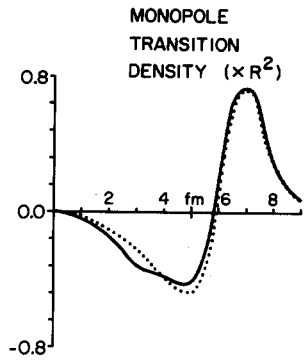

Fig. 10. Monopole transition density in ^{208}Pb. The solid curve is the result for the transition density operator $R^2 \Sigma_i \rho(r_i - R)$, for the SkI interaction between the ground and the 20 MeV state. Units are $\pi\,\mathrm{fm}^{-1}$. The dotted curve is the prediction of the Tassie model, eq. (43b). Here, the overall magnitude of the curve has no significance.

example is shown in fig. 9, where the ^{208}Pb giant $L = 2$ transition density is compared to the collective model. Blomqvist [8] displays the transition density of the $L = 3$ state in ^{208}Pb; this too is very close to the collective model.

There have been two collective models proposed for the monopole, a hydrodynamic model [73], which has a transition density proportional to a Bessel function, and the model of uniform breathing motion [23], which has the transition density (43b). The computed transition density in ^{208}Pb is very close to the breathing model, as may be seen from fig. 10. We can understand from this transition density why the interaction lowered the energy of the monopole state. Even though it has a radial node, the transition density is peaked on the surface: the density change is greater at the radius of the surface during the breathing motion. The interaction is always attractive in this region, hence the state is lowered in energy.

The isovector excitation, which gave difficulty with an unphysical split into two strong states, has an amusing aspect with the transition densities. There are two ourstanding collective models for the isovector dipole; the hydrodynamic Steinwedel–Jensen [46] model, for which the transition density is a Bessel function, and the Goldhaber–Teller model, which has a transition density satisfying eq. (43a). Both models are simulated in the RPA transition density [33]: the lower state follows the SJ model and the upper state the GT model.

10. Energy formulas

A compact summary of the mass dependence of resonance energies is often made with the parametrization

$$E = K/A^{1/3} \,. \tag{54}$$

However, there is also motivation from eq. (41) for a parametrization of the form,

$$E = K_{\mathrm{LT}}(n\hbar\omega) \tag{55}$$

Table 9
Peak positions of giant collective multipoles, expressed as coefficients of oscillator energies, eq. (55) and eq. (56). The range of variation from ^{40}Ca to ^{208}Pb is shown.

Multipole	K_{LT}(SkI)	K_{LT}(SkII)	Empirical	Other calculations
Isoscalar $L = 0$	1.5 – 1.6	1.25 – 1.45		1.2 (35)
$L = 2$	0.76 – 0.83	0.89 – 0.94	0.75	0.7 (72)
$L = 3$	0.30 – 0.45	0.45 – 0.55	0.31 – 0.38	
Isovector $L = 0$	2.1 – 2.4	2.2 – 2.5		2.1 (53)
$L = 1$	2.1 – 2.2	2.2 – 2.4	1.95	

where $\hbar\omega$ is some characteristic unperturbed energy of the system, for example the oscillator energy, and n is the number of energy quanta needed to create the L-multipole excitation in the oscillator model. In fact, we find that this parametrization allows a superior fit over the range ^{16}O–^{208}Pb, using oscillator energies determined from nuclear sizes [58]:

$$\hbar\omega = 45/A^{1/3} - 25/A^{2/3}. \tag{56}$$

The empirical and computed scaling factors K_{LT} are summarized in table 9. We note that the two isovector multipoles have nearly the same K_{LT}, and also the magnitude of the constant roughly accords with eq. (41). No such simple behavior is evident in the K_{20} and K_{30}. Comparing SkI and SkII with experiment, we do see that SkI agrees and SkII disagrees with the quadrupole data. We conclude that in general SkI is superior to SkII in describing the giant resonances.

11. Low-lying states

The prediction of the theory for the low-lying collective states will now be examined in some detail. To determine the energies of these states, the poles of the Green's function are located by an energy search with ω nearly real. The cases in which a pole is found in reasonable correspondence to the lowest physical state of a given multipolarity are listed in table 10. We have left out of the table the 2^+ states in nuclei with low-lying 0^+ states; such states are probably based more

Table 10
Energies of low-lying states (MeV).

L^π	Nucleus	Experimental	SkI	SkII
2^+	^{208}Pb	4.07	5.4	5.2
3^-	^{16}O	6.13	6.2	7.5
	^{40}Ca	3.74	3.3	5.1
	^{90}Zr	2.74	2.6	3.9
	^{208}Pb	2.61	2.7	3.2
4^+	^{208}Pb	4.31	5.4	6.4
5^-	^{40}Ca	4.48	5.4	7.5
	^{208}Pb	3.2	3.3	4.6

Table 11
Electromagnetic transition rates ($0 \to L$) for low-lying states expressed in Weisskopf units, eq. (57).

L^π	Nucleus	Experimental (ref.)	SkI	SkII
2^+	^{208}Pb	8 [75]	7	7
3^-	^{16}O	14 [76]	4	8
	^{40}Ca	25 [77, 79]	11	19
	^{90}Zr	32 [74]	28	57
	^{208}Pb	39.5 [75]	29	50
4^+	^{208}Pb	15 [78]	7	4
5^-	^{40}Ca	10 [77], 30 [79]	3	8
	^{208}Pb	14 [75]	6	16
6^+	^{208}Pb		5	9

on the excited 0^+ than on the ground Hartree–Fock configuration. It was found necessary to include the single-particle Coulomb energies in ^{208}Pb; without the Coulomb field on the protons, the 3^- state is higher in excitation. On the whole, we see that the SkI prediction is usually within 20% of the empirical state and errs on the high side. SkII, on the other hand, uniformly predicts states at too high an excitation energy. This is consistent with the extreme velocity-dependence of SkII. Previous calculations of vibrational states have mostly resorted to adjustment of the interaction potential to reproduce the correct or close energies [59–61, 22]. The successful calculations of Kuo [43] have as their ingredients empirical single-particle energies, realistic interactions, and screening of the particle–hole interaction. Use of empirical rather than Hartree–Fock single-particle energies tend to make excitation energies smaller [62]. On the other hand, the screening interaction is a repulsive effect which pushes the collective states back up in energy.

Let us now examine the electromagnetic transition rates for the low states. Since our main calculations were with an isoscalar operator set, we determined the relative strength of neutron and proton excitation by a separate calculation, and then scaled the results accordingly to get electromagnetic rates. These are given in table 11, expressed in Weisskopf units, S_W,

$$B(\mathrm{E}L: 0 \to L) = e^2 S_W \left(\frac{2L+1}{4\pi}\right)\left(\frac{3}{3+L}\right)^2 (1.2A^{1/3})^{2L} . \tag{57}$$

It is possible to see some pattern in the results. The two interactions usually differ by a factor of two, with SkII predicting stronger transition strengths. However, in the ^{208}Pb 2^+, the predictions agree with each other and with experiment. Often in other cases the predictions bracket the experimental transition rate. The close agreement possible for the ^{208}Pb 3^- has been noted in earlier calculations [8, 42]. Two anomalies that stand out are the 3^- in ^{16}O and the 4^+ in ^{208}Pb. In ^{16}O, our configuration space is large enough to contain virtually all of the energy-weighted sum rule, but end up with a small transition rate. The early calculation of Gillet and Vinh Mau [59] also predicts a small transition rate, of the same magnitude as our SkII result. As an example of possible effects which could be responsible for the poor showing of the Hartree–Fock model in ^{16}O, alpha particle clustering would give some $L = 3$ deformation to the ground state and enhance the transition rate. The 4^+ in Pb is equally puzzling; our configuration space contains 92% of the energy-weighted sum rule, and extension of the space has negligible

effect on the prediction. The energy of our state is also off here by 40%, and one could well ask whether the high-momentum components of the interaction are simply too weak in the Skyrme models. A similar difficulty with the 4^+ was found in the more phenomenological calculation of Ring and Speth [22].

12. Inelastic scattering

As an application of the response function technique, we shall consider the differential cross section for inelastic scattering of various projectiles. Normally cross sections are analyzed by either isolating individual states and comparing with a microscopic theory of that state, or by looking at the entire spectrum and comparing with a quasi-elastic theory. We shall concentrate on the overall spectrum, summed over all angular momentum transfers. We can compare this both with experiment and with the cruder quasi-elastic models.

The first reaction to be considered is inelastic electron scattering. The electron is the simplest probe from a theoretical point of view, because its coupling to the nucleons is well known, and the Born approximation is at least reasonable. The cross section for a momentum transfer q and energy loss E is well approximated by the equation

$$\frac{d\sigma}{d\Omega} = \frac{F^2}{Z^2} \left.\frac{d\sigma}{d\Omega}\right|_{\text{Mott}} \tag{58}$$

where

$$F^2 = \sum_i |\langle 0| \sum_{\text{protons}} e^{iq'\cdot r} |i\rangle|^2 \, \delta(E_i - E)$$

and q' is the momentum transfer in the vicinity of the nucleus, which differs from q by Coulomb effects. Our normalization, in case there is any ambiquity, is such that $F^2 = Z^2$, the square of the charge, for elastic scattering with $q' = 0$. The factor F^2 can obviously be computed in the response function formalism as [2]

$$F^2 = 4\pi \sum_L \frac{(2L+1)}{\pi} \operatorname{Im}\left\langle j_L(q'r) \left(\frac{1+\tau_z}{2}\right) G j_L(q'r) \left(\frac{1+\tau_z}{2}\right)\right\rangle . \tag{59}$$

We have calculated this quantity for operator set C of table 7. In fig. 11 is displayed the strength as a function of energy and momentum transfer. The energy averaging interval is 1 MeV. It may be seen that bumps in the curves remain pronounced up to about 20 MeV in excitation. Where the bump is due to some particular angular momentum, we identify it as such. The positions are not precisely the same as in the previous sections, due to the limitations of the operator set C.

A question we can now address ourselves to is, how good is the Fermi gas model for describing the total strength function? The response in this model is familiarly called quasi-elastic scattering, and it has often been used to describe smooth backgrounds. In it, the strength function is proportional to the imaginary parts of the Lindhard function (see eq. (34)). This may be conveniently expressed as

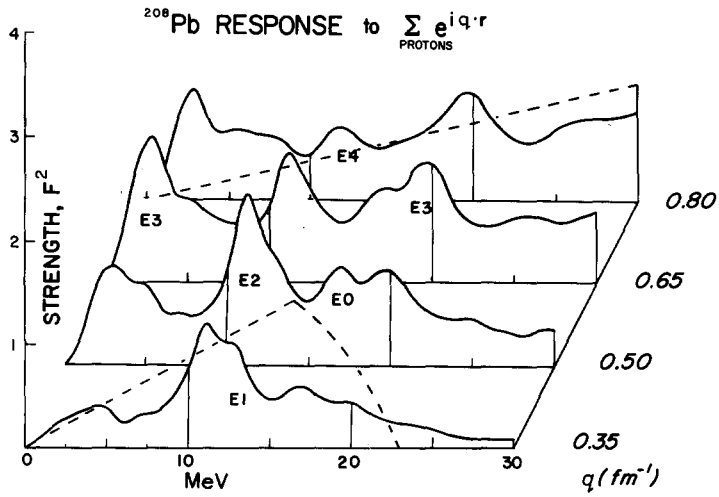

Fig. 11. Response of ^{208}Pb to an electromagnetic probe. The four graphs show eq. (59) for momentum transfers of 0.35, 0.50, 0.65, and 0.80 fm^{-1}, with an averaging interval $\Gamma = 1.0$ MeV. Dashed curves are the predictions of the quasi-elastic model, eq. (60).

$$F^2 = \frac{1}{\pi}\,\mathrm{Im}\,G^{(0)}(q,\omega) = \begin{cases} \dfrac{3Zm^2\omega}{2\hbar^3 q k_F^2} & \text{for } \hbar\omega < \dfrac{\hbar^2}{m}|2qk_F - q^2| \text{ and } q < 2k \\ \dfrac{3Zm}{4\hbar^2 q k_F}\left\{1 - \left(\dfrac{m\omega}{\hbar q k_F} - \dfrac{q}{2k_F}\right)^2\right\} & \text{for } \dfrac{\hbar^2}{m}|q^2 - 2qk_F| < \hbar\omega < \dfrac{\hbar^2}{m}|q^2 + 2qk_F| \end{cases} . \tag{60}$$

Obviously, this model does not give a useful approximation for low momentum transfer, $q < 0.5$ fm^{-1}. Not only do sharp resonances dominate this region, but a considerable fraction of the strength is in the spurious state. However, the mean energy of the strength function does roughly correspond to the Lindhard function, as may be seen in fig. 11, where we have plotted eq. (60) for momentum transfers of 0.35 and 0.8 fm^{-1}. It appears that the interactions and single-

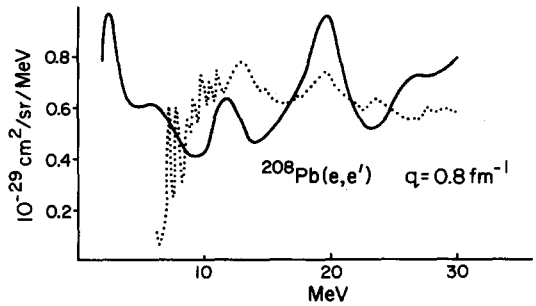

Fig. 12. Cross section for ^{208}Pb(e, e') at 250 MeV incident energy and 35° scattering angle according to eqs. (58) and (59). The experimental data is from the graph in ref. [40].

particle shell structure do not become negligible perturbations on the strength function until much higher q. For extremely high momentum transfers, $q \approx 2.5$ fm^{-1}, the Fermi gas model is seen to work quite well [63], when some corrections having to do with an effective mass are incorporated into the model. Experimental data at lower momentum transfer has recently been published by Nagao and Torizuka [40]. One of their curves is shown in comparison with our $|q| = 0.8$ fm^{-1} calculation in fig. 12. There is a rough correspondence in overall magnitude of the cross section, and a lesser correspondance between positions, shapes, and sizes of bumps. Below 11 MeV there is much more structure than our model would predict, even with a fine averaging interval. The theoretical bump at 11 MeV is due mostly to $L = 4$; Nagao and Torizuka assign their nearby peaks to $L = 2$ and $L = 1$. They also note an $L = 3$ peak at 19 MeV, and indeed our bump in this region is $L = 3$ (see fig. 6) together with some $L = 2$.

Inelastic scattering with other projectiles also provides useful data on the response function, but is less informative than electron scattering for two reasons. First, the Born approximation is not valid, both because the projectile wavefunction is strongly altered and because the nucleus does not respond linearly to the large fields made by the projectile. The best that can be done at present time for the description of the reaction is the Distorted–Wave Born Approximation (DWBA). Nonlinearities in the response in principle can be treated by higher-order Born approximations, but existing calculational schemes are unreliable or cumbersome or both. Second, the interaction between projectile and nucleon in the nucleus is not known as well as desired. However, successful models for the excitation of low-lying collective states have been made with the macroscopic method (outlined below), realistic interactions [64], or even the Skyrme interaction [65].

Besides the questions of principle a purely technical problem remains, in that the existing DWBA codes require a nuclear transition density as input, i.e. G is forced to be of the form (42). The codes do not provide a scattering transition density analogous to the Bessel functions of electron scattering. So for our nuclear transition density we shall assume the following,

$$\langle 0|\hat{\rho}(r)|L\rangle = C \left.\frac{\mathrm{d}\rho_0}{\mathrm{d}r}\right|_r Y_M^L(\hat{r}) . \tag{61}$$

As noted earlier, this is actually an excellent approximation for the collective states. Later we shall investigate the magnitude of corrections due to parts of the Green's function missed with eq. (61).

The macroscopic model has recently been applied by Satchler [66] to the giant guadrupole and dipole states. Details of the theory are given in ref. [67]; only the essential equations will be presented below. We first evaluate the coefficient C in eq. (61) by requiring that the response to the perturbation $(\mathrm{d}\rho_0/\mathrm{d}r)|_r$ be given correctly. This yields

$$C = \left[\int \left(\frac{\mathrm{d}\rho_0}{\mathrm{d}r}\right)^2 r^2\,\mathrm{d}r\right]^{-1} \sqrt{\frac{1}{\pi}\int \mathrm{d}E\ \mathrm{Im}\left\langle \frac{\mathrm{d}\rho_0}{\mathrm{d}r}\ G\ \frac{\mathrm{d}\rho_0}{\mathrm{d}r}\right\rangle}. \tag{62}$$

If both the transition potential and the central optical potential are given by convolutions of an interaction and a density, then eq. (61) implies the specific transition potential given by

$$\langle 0|V|L\rangle = Y_M^L \frac{\mathrm{d}V_0}{\mathrm{d}r} \frac{\sqrt{(1/\pi)\int \mathrm{d}E\ \mathrm{Im}\langle(\mathrm{d}\rho_0/\mathrm{d}r)\, G(\mathrm{d}\rho_0/\mathrm{d}r)\rangle}}{\int (\mathrm{d}\rho_0/\mathrm{d}r)^2\, r^2\,\mathrm{d}r}. \tag{63}$$

DWBA codes such as DWUCK permit use of transition potentials of this form, the standard notation being

$$\langle 0|V|L\rangle = Y_M^L \frac{\beta_L}{\sqrt{2L+1}} R_0 \frac{dV_0}{dr} \tag{64}$$

and $d\sigma/d\Omega = \beta_L^2 (d\sigma/d\Omega)^L_{\mathrm{DWBA}}$ with $(d\sigma/d\Omega)_{\mathrm{DWBA}}$ the output of the computer code in the macroscopic model. Thus in our model β_L is given by

$$\beta_L^2 = (2L+1)\frac{1}{\pi}\int dE\, \mathrm{Im}\left\langle \frac{d\rho_0}{dr} G \frac{d\rho_0}{dr}\right\rangle \Big/ R_0^2 \left[\int \left(\frac{d\rho_0}{dr}\right)^2 r^2\, dr\right]^2 \tag{65}$$

and the differential cross section is

$$\frac{d\sigma}{d\Omega\, dE} = \sum_L \frac{(2L+1)\,\mathrm{Im}\langle (d\rho_0/dr)\, G(d\rho_0/dr)\rangle_L}{\pi R_0^2 [\int (d\rho_0/dr)^2 r^2\, dr]^2} \times \left(\frac{d\sigma}{d\Omega}\right)^L_{\mathrm{DWBA}} . \tag{66}$$

The reaction we consider is ^{208}Pb (p, p'). The scalar part of the proton–nucleus interaction is taken as eq. (63), with a standard optical potential [68] for V_0. For the spin and isospin parts of the interaction, we assume that the interaction has a Serber exchange mixture, which implies that each nonscalar component has $\frac{1}{3}$ the magnitude of the scalar interaction. As mentioned earlier, the spin-dependent Skyrme interaction is unreasonable, so we just use $G^{(0)}$ for the nuclear model in this channel. In any case, the scalar response dominates at all energies, so the details here are not important.

The results for the cross section of 62 MeV protons at 20° are shown in fig. 13 as the solid line, to be compared with the data of Bertrand and Peelle [69] on ^{209}Bi. The experimental data is in 1 MeV bins, and we used a 0.5 MeV averaging interval in the calculation. Angular momentum transfers up to $L = 9$ are included, which just covers the range of angular momentum transfer that make a significant contribution. The lowest state, the 3^-, is within 10% agreement, as it should be from the known consistency between electromagnetic transition strengths and inelastic scattering strengths. For higher excitation energies, the model does very poorly indeed: the ex-

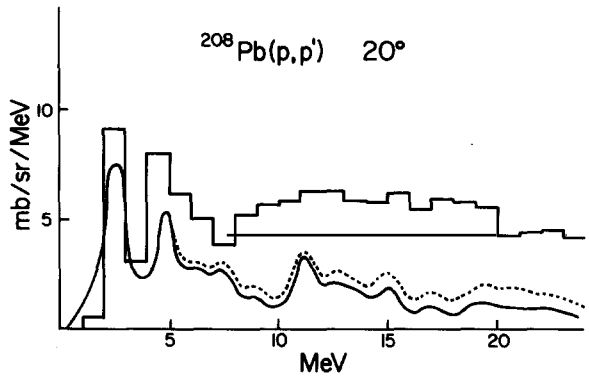

Fig. 13. Cross section for ^{208}Pb(p, p') at 62 MeV and 20°. Solid line is theory for the macroscopic transition density; dashed line has an incoherent contribution added from a transition density 1 fm further from the surface. Experimental data is for ^{208}Bi, from ref. [69].

perimental cross section is much larger than theory. Troubles begin with the experimental peak near 4 MeV due to 4^+ and 6^+, which, as mentioned earlier, the RPA model fails to explain. The giant quadrupole state, which is an isolated feature in the theory even with all other multipoles added on, appears experimentally as a small bump on a large background.

In an effort to understand the background within the framework of the model, we have examined more carefully the radial distribution of transition densities. A similar reaction ^{208}Pb (α, α'), also has a large cross section which has been explained by knockout of a nucleon [70]. The knockout process is of course implicit in the response function, but it has a transition density which peaks much further out in the surface. A graph of such a transition density is given in ref. [55]. The inelastic scattering process enormously favors the external region, so the macroscopic calculation could be quite inaccurate. We have examined this hypothesis by adding to the transition density a term peaked 1 fm further away from the surface. To avoid double-counting it is orthogonalized to the macroscopic transition density,

$$\langle 0|\hat{\rho}(r)|L\rangle_{\text{ext}} = C' \left.\frac{\mathrm{d}\rho_0}{\mathrm{d}r}\right|_{(r-1)\text{fm}} - \left\langle \frac{\mathrm{d}\rho_0}{\mathrm{d}r}(r+1)\frac{\mathrm{d}\rho_0}{\mathrm{d}r}\right\rangle \frac{\mathrm{d}\rho_0}{\mathrm{d}r} \Big/ \left\langle \frac{\mathrm{d}\rho_0}{\mathrm{d}r}\frac{\mathrm{d}\rho_0}{\mathrm{d}r}\right\rangle .$$

The strength for this density is an order of magnitude less than the "background" strength of the macroscopic model. However, the DWBA cross sections are four or five times larger at the larger distance, so the external region is indeed significant. We have also examined the internal region in a similar way, and find that it is completely negligible, due to projectile absorbtion. To quantatively estimate the knockout, it is desirable to use a microscopic interaction in this low density region instead of the macroscopic V_0. A δ-interaction of strength 400 MeV-fm^3 corresponds to a V_0 of -64 MeV; using this we find that the external region is nearly as important as the surface in generating a background. The sum is shown as the dashed curve in fig. 13. While our calculation is far from precise, it appears that the knockout process still does not account for the remainder of the cross section. This is further supported by a more refined calculation [80]. In view of the much better agreement with electron scattering, a reasonable conclusion is that much of the background is due to multiple excitation processes.

13. Conclusion

We have found response function technique is very useful as a theoretical and numerical tool. Some of the calculations presented, especially the inelastic scattering in the continuum, would have been very tedious by the standard method. However, we also found that some effort and operator truncation was required to make the method numerically manageable in the presence of velocity-dependent interactions. For the simpler operator sets, the method is very fast. Also the form of the output, and integral of the strength function in coordinate space, is close to what is needed for comparison of theory and experiment.

Turning to the specific Hartree–Fock models, we find that on the whole, the RPA and empirically-based Skyrme interaction provides a useful theory of nuclear excitations. Low-lying states and gross features are fairly insensitive to the specific interaction, and agreement with experiment is often close. The two interactions we tested, SkI and SkII, did however show systematic differences in their predictions, with SkI favored by most features, such as the positions of levels,

and mean energies of strength functions. However, often SkI did quite poorly on the transition strength of low-lying states. In several of these cases SkII did better, but on the whole, SkI gives a better description of the dynamics.

The results seem encouraging enough that the model would profitably be applied to other problems of nuclear physics that have not been considered here. For example, the theory of the imaginary optical potential is closely tied to the strength function for nuclear excitation. Another problem is the description of the interaction between nucleons in the nucleus. This requires a good understanding of the polarization of the nucleus by the field of an individual nucleon. Up to the present, treatment of the polarization has been extremely cumbersome; perhaps the response function technique will provide more reliable calculations or better insight.

Acknowledgement

We wish to thank K.F. Liu for pointing out the nonvanishing interaction contributions to the sum rules. Also, this work would not have been completed without the Cyclotron Laboratory's computer facility.

References

[1] A. Fetter and S. Walecka, Quantum Theory of Many-Particle Systems (McGraw-Hill, N.Y., 1971).
[2] W. Czyz and K. Gottfried, Ann. Phys. 21 (1963) 47.
[3] R.A. Ferrell, Phys. Rev. 107 (1957) 1631.
[4] M. Baranger, Phys. Rev. 120 (1960) 957.
[5] G. Brown, J. Evans and D. Thouless, Nucl. Phys. 24 (1961) 1.
[6] D.J. Thouless, Nucl. Phys. 22 (1960) 78.
[7] M. Weigel, L. Garside and P. Haug, Phys. Rev. C3 (1971) 563.
[8] J. Blomqvist, Phys. Letters 28 (1968) 22.
[9] D. Vautherin and D. Brink, Phys. Rev. C5 (1972) 626.
[10] S. Moszkowski, Phys. Rev. C2 (1970) 402.
[11] J. Negele and D. Vautherin, Phys. Rev. C5 (1972) 1472.
[12] A.M. Lane, Nuclear Theory (Benjamin, N.Y., 1964) p. 107.
[13] G. Baym and L. Kadanoff, Phys. Rev. 124 (1961) 287.
[14] T. Skyrme, Nucl. Phys. 9 (1959) 615.
[15] J. Eisenberg, B. Spicer and M. Rose, Nucl. Phys. 71 (1965) 273.
[16] A. Bohr and B. Mottelson, Nuclear Structure (Benjamin, N.Y., 1969).
[17] J. Lindhard, Kgl. Danske Vid. Selsk. Mat. Fys. Med. 28 (1954) no. 8.
[18] G.E. Brown, J.H. Gunn and P. Gould, Nucl. Phys. 46 (1963) 598.
[19] G. Jacob and Th.A.J. Maris, Rev. Mod. Phys. 45 (1973) 6.
[20] G. Saunier et al., Can. J. Phys. 51 (1973) 629.
[21] S.O. Bäckman, Nucl. Phys. A120 (1963) 593.
[22] P. Ring and J. Speth, Phys. Letters 44B (1973) 477;
S. Krewald and J. Speth, Phys. Letters 52B (1974) 295.
[23] L.J. Tassie, Aust. J. Phys. 9 (1956) 407.
[24] G. Bertsch, Ann. Phys. 86 (1974) 138.
[25] S. Fallieros, Proc. Sendai Conf., 1972, Supplement to research report of Laboratory of Nuclear Science, Tokohu Univ. Vol. 5 (1972) p. 185.
[26] N. Auerbach, Phys. Letters 36B (1971) 293.
[27] J.V. Noble, Ann. Phys. (New York) 67 (1971) 98.
[28] J. Ahrens et al., ref. [25] p. 213.

[29] A. Veyssiere et al., Nucl. Phys A159 (1970) 561.
[30] R. Bergere, private communication.
[31] W. Weng, T. Kuo and G. Brown, Phys. Letters 46B (1973) 329;
M. Finck et al., Phys. Letters 49B (1974) 20.
[32] G.F. Bertsch, Phys. Rev. Letters 31 (1973) 121.
[33] G. Bertsch and S.F. Tsai, Phys. Letters 50B (1974) 319.
[34] J. Damgaard et al., Nucl. Phys. A121 (1968) 625.
[35] S. Wong, G. Saunier and B. Rouben, Nucl. Phys. A169 (1971) 294.
[36] R. Sharp and L. Zamick, Nucl. Phys. A208 (1973) 130.
[37] G.E. Brown, in: Facets of Physics, eds. Bromley and Hughes (Academic Press, N.Y., 1970) p. 141.
[38] M. Lewis and F. Bertrand, Nucl. Phys. A196 (1972) 337.
[39] A. Moalem, W. Beneson and G. Crawley, Phys. Rev. Letters 31 (1973) 482.
[40] M. Nagao and Y. Torizuka, Phys. Rev. Letters 30 (1973) 1068.
[41] L. Rutledge and J. Hiebert, Phys.Rev. Letters 32 (1974) 551.
[42] B. Mottelson, Private communication from R. Broglia.
[43] T. Kuo, J. Blomqvist and G.E. Brown, Phys. Letters 31B (1970) 93.
[44] J.P. Elliott and B.H. Flowers, Proc. Roy. Soc. (London) A242 (1957) 57.
[45] G. Brown and M. Bolsterli, Phys. Rev. Letters 3 (1959) 472.
[46] H. Steinwedel, J. Jensen and P. Jensen, Phys. Rev. 79 (1950) 1019.
[47] M. Goldhaber and E. Teller, Phys. Rev. 74 (1948) 1046.
[48] S. Perez, Phys. Letters 33B (1970) 317.
[49] J. Speth, Villars Winter Meeting, 1974.
[50] M. Danos and W. Greiner, Phys. Rev. B138 (1965) 876.
[51] G. Bertsch, Phys. Letters 37B (1971) 470.
[52] C. Dover, R. Lemmer and F. Hahne, Ann. Phys. 70 (1972) 458.
[53] A. Bohr, J. Damgaard and B. Mottelson, in: Nuclear Structure, ed. Hossain (North-Holland, Amsterdam, 1967) p. 1.
[54] A. Z. Mekjian, Phys. Rev. Letters 25 (1970) 888.
[55] N. Auerbach and G. Bertsch, Phys. Letters 43B (1973) 175.
[56] S. Hanna et al., Phys. Rev. Letters 32 (1974) 114.
[57] K. Snover et al., Phys. Rev. Letters 32 (1974) 317.
[58] J. Blomqvist and A. Molinari, Nucl. Phys. A106 (1968) 545.
[59] V. Gillet and N. Vinh Mau, Nucl. Phys. 54 (1964) 321.
[60] V. Gillet and E. Sanderson, Nucl. Phys. 54 (1964) 472.
[61] V. Gillet, A. Green and E. Sanderson, Nucl. Phys. 88 (1966) 321.
[62] G. Bertsch and T. Kuo, Nucl. Phys. A112 (1968) 204.
[63] E. Moniz et al., Phys. Rev. Letters 26 (1971) 445.
[64] F. Petrovich et al., Phys. Rev. Letters 22 (1969) 895.
[65] K. Davies and G. Satchler, Nucl. Phys. A222 (1974) 13.
[66] G. Satchler, Nucl. Phys. A195 (1972) 1.
[67] N. Austern, Direct Reaction Theory (Wiley, N.Y., 1969) p. 126.
[68] F. Becchetti and G. Greenlees, Phys. Rev. 182 (1969) 1190.
[69] F. Bertrand and R. Peelle, Oak Ridge Report ORNL-4638 (1971); Phys. Rev. C8 (1973) 1045.
[70] N. Chant and E. Henley, Phys. Rev. Letters 27 (1971) 1657.
[71] Baumgärtner and Schuck, Kernmodelle.
[72] T. Suzuki, Nucl. Phys. A217 (1973) 182.
[73] J.D. Walecka, Phys. Rev. 126 (1962) 653.
[74] J. Bellicard et al., Nucl. Phys. A143 (1970) 213.
[75] J. Ziegler and G. Peterson, Phys. Rev. 165 (1968) 1337.
[76] T. Alexander and K. Allen, Can. J. Phys. 43 (1965) 1563.
[77] J. Heisenberg et al., Nucl. Phys. A164 (1971) 353.
[78] M. Nagao and Y. Torizuka, Phys. Letters 37B (1971) 383.
[79] K. Itoh, M. Oyamada and Y. Torizuka, Phys. Rev. C2 (1970) 2181.
[80] S.F. Tsai and G.F. Bertsch, Phys. Rev. C11 (1975) to be published.